The Jaws, Oral Cavity, and Nasopharynx

10

Christos Angelopoulos and William C. Scarfe

Contents

C. Angelopoulos, D.D.S., M.S. (✉)
Aristotle University of Thessaloniki,
Thessaloniki, Greece

Columbia University, College of Dental Medicine,
New York City, NY, USA
e-mail: angelopoulosc@gmail.com

W.C. Scarfe, B.D.S., F.R.A.C.D.S., M.S.
Division of Radiology and Imaging Science,
Department of Surgical/Hospital Dentistry,
University of Louisville School of Dentistry,
Louisville, KY, USA
e-mail: william.scarfe@louisville.edu

10.1 Introduction

Maxillofacial cone beam computed tomographic (CBCT) images pose difficulties for many dental professionals because most are unfamiliar with developing and interpreting the image formats developed from the CBCT volume—they are like no other images previously available in the dental diagnostic imaging arsenal. This becomes even more challenging when evaluating tomographic images of the maxillofacial region due to the anatomical complexity of this area.

For years dental professionals have been trained in utilizing and interpreting traditional plain film dental imaging modalities, such as intraoral radiography, panoramic radiography, and cephalometric radiography, and are well aware of the advantages, indications, and contraindications for their use. Clinicians are also cognizant of the limitations of these images in that they are two-dimensional representations of three-dimensional structures, superimposing various osseous structures, and subject to geometric effects (image magnification and distortion) due to the projectional nature of traditional imaging. As described previously, CBCT acquisition is entirely different in that multiple projective frame data are reconstructed to provide a volumetric dataset. Unlike 2D projective imaging, primary reconstruction demonstrates the dataset as stacks of uniform and contiguous

W.C. Scarfe, C. Angelopoulos (eds.), *Maxillofacial Cone Beam Computed Tomography*,
https://doi.org/10.1007/978-3-319-62061-9_10

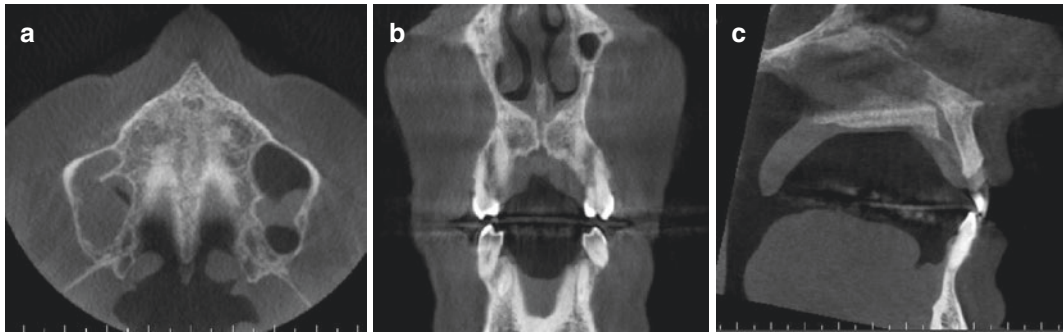

Fig. 10.1 Representative primary reconstruction of CBCT volumetric data as axial (**a**), coronal (**b**), and sagittal (**c**) orthogonal displays

sections in the three orthogonal planes (axial, coronal, and sagittal) (Fig. 10.1). Subsequently the volume can be sectioned and reconstructed in any possible plane, either linearly or obliquely providing a flat oblique or curved planar image, respectively (Scarfe et al. 2010). This property is known as *multiplanar imaging/reformatting* (MPR).

MPR is the capability to re-synthesize a multitude of images or sections with simple functions of data manipulation after a volume has been acquired. This function completely eliminates the superimposition of the anatomical structures or even pathology encountered with conventional imaging modalities, markedly increasing the diagnostic efficiency of CBCT (Angelopoulos 2008). MPR is most often used in combination with trans-axial imaging—multiple limited field of view (FOV) thin section contiguous slicing orthogonal to the MPR plane providing multiple cross sections. This additional display tool is perhaps the most useful in maxillofacial interpretation as it allows representation of features according to their anatomical orientation and eliminates the superimposition of adjacent structures with the control of MPR slice thickness. However, the application MPR may be challenging as it provides a sequence of multiple image sequences with unobscured detail and demands a higher level of professional competence than that necessary to interpret a single projective image. The diagnostic yield from orthogonal and MPR displays is dependent upon:

1. The knowledge, experience, and technical skill of the diagnostician in developing reconstructed images.
2. The correct application of the available MPR format.
3. Sound knowledge of the anatomy and interrelationships of elements within the region of interest.

In clinical practice, anatomical knowledge is perhaps the most demanding factor for successful interpretation since the maxillofacial skeleton is composed of numerous complex structures which form multidirectional spatial relationships with one another. Consequently, structural appearance will vary considerably in different tomographic planes (Angelopoulos 2014). Familiarity with the variable tomographic appearance of the maxillofacial structures and their spatial relationships is crucial in understanding the difference between diseased tissues and anatomical variants of the maxillofacial skeleton, disease origin and disease spread.

The goal of this chapter is to review maxillofacial anatomical structures and common variations which may be represented on CBCT images.

10.1.1 The Role of Reformatted Panoramic Imaging

Although review of orthogonal planar imaging (axial, coronal, and sagittal sections) is important for maxillofacial diagnosis, curved planar MPR reformatting with perpendicular trans-axial

(cross-sectional) imaging of the maxilla and the mandible seems to be the most commonly used in maxillofacial CBCT applications. This is because MPR provides optimal imaging of the jaws as the curved plane conforms to the uniqueness of the jaw shape. Panoramic reformation is accompanied by creation of a series of sequential, cross-sectional images perpendicular to jaw which provide an "in depth assessment" of a certain region of the jaw. The combination of both formats negates the superimposition of anatomic structures inherent in 2D dental imaging. Moreover, it provides accurate representation of the alveolar ridge height and width that is crucial in specific treatment options especially in surgical procedures (Scarfe et al. 2006). Panoramic image creation is an integral part of most CBCT viewing software. It is mandatory that different panoramic reformats be generated for the maxilla and mandible when accurate measurements are required due to curvature differences of the two jaws (Figs. 10.2 and 10.3). In this way, parallax error will be minimized and measurements obtained of the residual alveolar ridge of edentulous areas the cross-sectional images for alveolar bone height and width will be the most accurate.

Cross-sectional imaging of the jaws provides information and details concerning:

- The shape, size, dimensions, and angulation of the edentulous alveolar ridge (Fig. 10.4). Although variations in the shape and size of the mandibular alveolar bone exist among dentate individuals, it is the residual alveolar ridge that undergoes the most changes with time due to resorption, after tooth extraction. Bone atrophy may alter the spatial relationship of the structures of concern and may add to the anatomical limitations in certain treatment options, especially in the placement of dental implants.

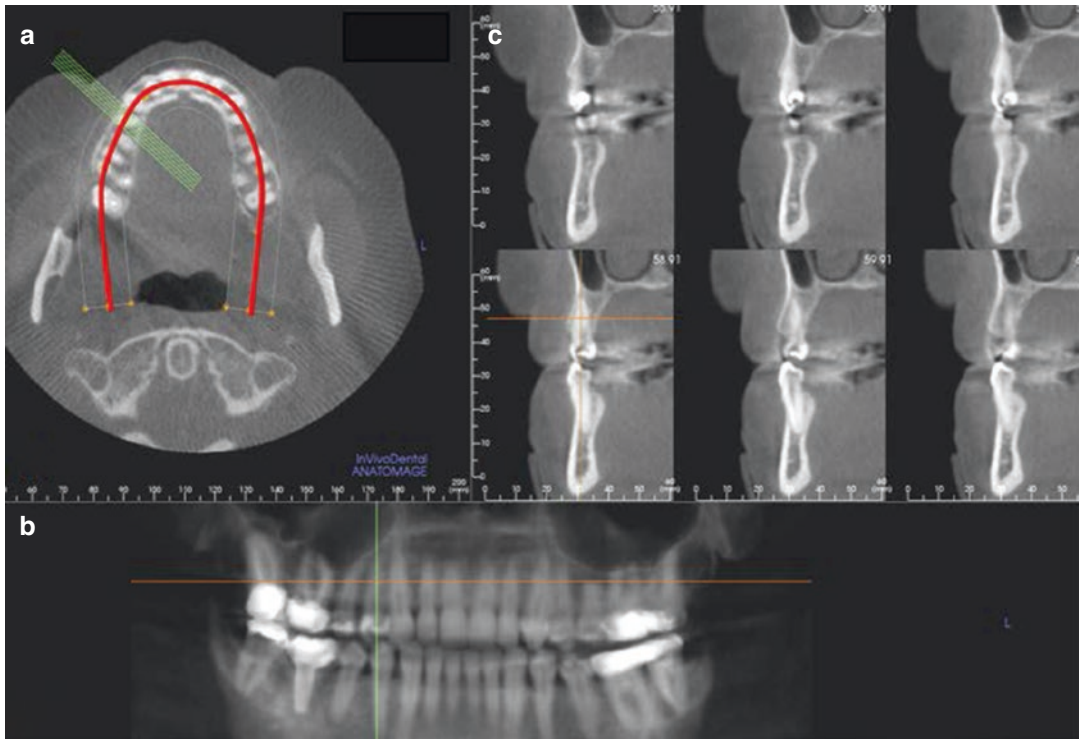

Fig. 10.2 The axial image (**a**) is used to create a "spline" at the mid-root level of the teeth along the arch shape of the maxilla from which a curved planar "panoramic" image (**b**) is reformatted. The *curvilinear line* (*red*) represents the center of the panoramic image. The *green lines*, perpendicular (or near perpendicular) to the *curvilinear line*, represent the reformatted cross sections (**c**) in the region of interest (maxillary right premolars). For accurate dimensions of the maxillary bone in cross section, the *green lines* (cross-sectional images) should be perpendicular to the maxillary bone

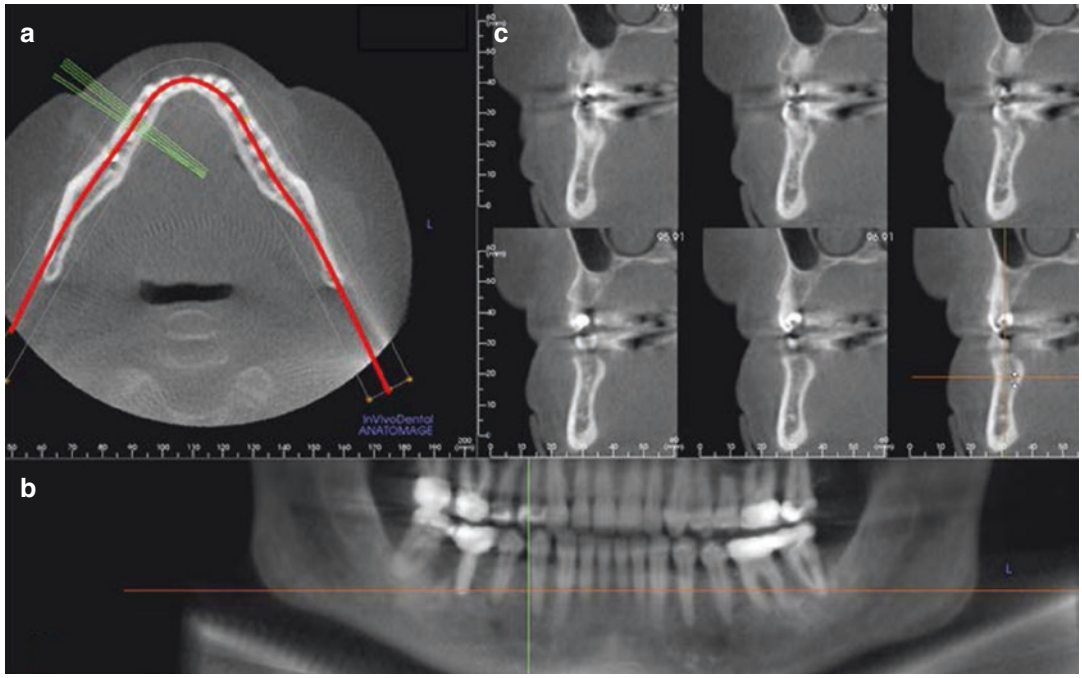

Fig. 10.3 Panoramic reformat of the same individual as Fig. 10.2 except that the "spline" is developed on an axial image (**a**) at the root apex level of the mandibular teeth along the arch shape of the mandible. Note that the reformatted panoramic image (**b**) and cross-sectional images (**c**) demonstrate the same anatomy in the right premolar region of the jaws somewhat differently

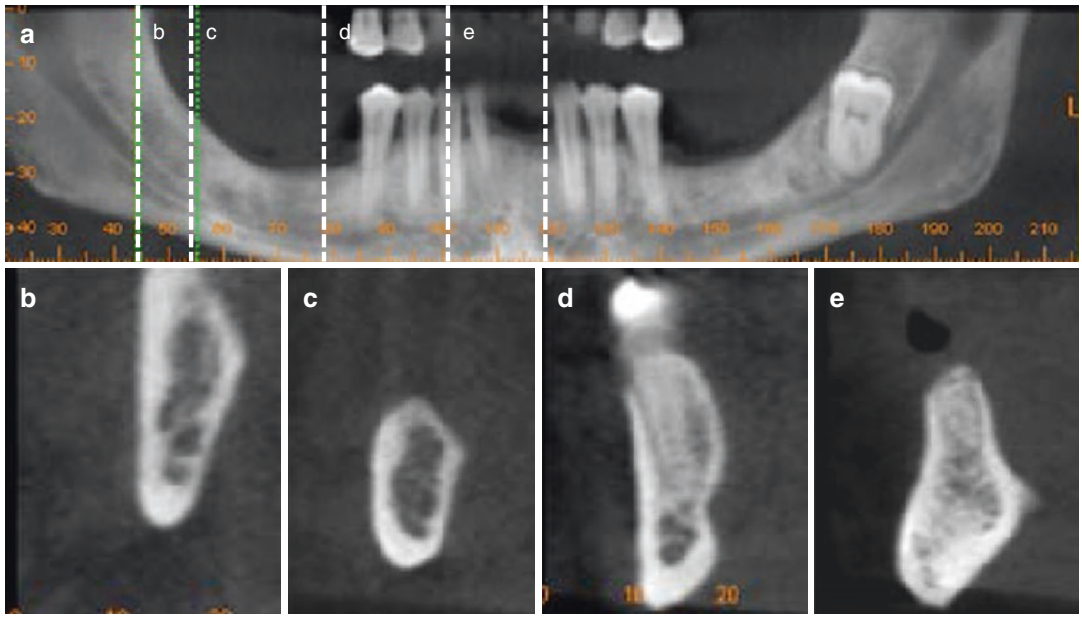

Fig. 10.4 Reference panoramic image (**a**) with a series of cross sections of the right mandible extending from the retromolar trigone (**b**) to the molar area (**c**) to the premolar area (**d**) and finally to the anterior mandible (**e**). The region from which each of the representative cross-sectional images is taken is shown by the *dotted white lines* on the panoramic image (**a**). Note the gradual changes in the shape and size of the mandibular bone from the posterior to anterior locations. Anatomical variation of the shape and size of the mandibular bone is very common

- The spatial relationship of the anatomical structures in the jaws that are routinely encountered in intraoral and panoramic images.
- The long axis of the alveolar bone and the related long axis of the teeth in the region which do not necessarily coincide (Fig. 10.5). This is an important information needed during dental implant treatment planning.

10.1.2 A Panoramic Approach to Regional CBCT Anatomy

For maxillofacial CBCT imaging, reformatted panoramic in combination with serial trans-axial (cross-sectional) images are the images of choice for the evaluation of the maxillary and mandibular dental arches including the dentition as well as the associated alveolar bone in edentulous regions. However, frequently, other reconstructions may be developed to assess the anatomic region from different perspectives including standard orthogonal multiplanar sections (axial, coronal, and sagittal), other region specific planar or curved planar MPR sections, and surface rendering reconstructions. For example, coronal sections provide a wider view of the maxillary and mandibular inter-arch relationships and more accurately demonstrate the spatial relationships of these structures.

Knowledge of the anatomic regions and specific topographic anatomy seen on reformatted panoramic images is essential to identify and describe the location of specific features or anomalies. However, differences between the

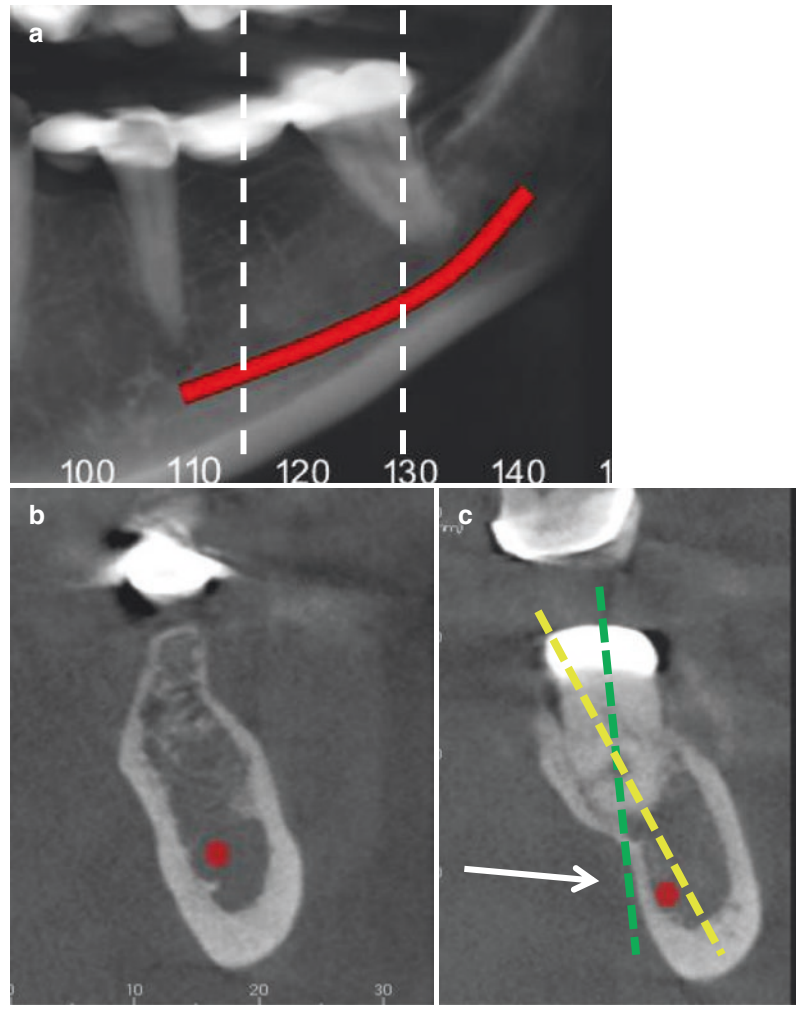

Fig. 10.5 Cropped panoramic image (**a**) and mandibular cross sections (**b**, **c**) in the molar region at the corresponding *dashed lines* in the panoramic image. The long axis of the mandibular bone (*yellow dashed line*) frequently does not correspond to the long axis of the teeth in the region (*green dashed line*). The faint low-density area indicated by the *white solid arrow* is the submandibular gland fossa (depression)

construction of reformatted panoramic images from CBCT data and production of conventional images from classical rotational panoramic radiography result in seemingly similar but, in many respects, different images (Table 10.1).

The process of creating a panoramic image also generates multiple trans-axial images perpendicular to the curved planar spline. Review of the volumetric data involving the jaws based on this reformation protocol is an essential radiologic skill for dental practitioners and involves a systematic approach and a detailed understanding of the anatomic features in each of six zones (Fig. 10.6). Three zones are in the midline and three zones are bilateral.

- **Zone 1**. Nasal fossa, nasopharynx (See Chap. 13), zygoma, maxilla, and maxillary sinuses (See Chap. 12).
- **Zone 2**. Temporomandibular joint (See Chap. 24) and temporal bone (See Chap. 14)
- **Zone 3**. Mandibular ramus, cervical vertebrae (See Chap. 11), oropharynx (See Chap. 13), and parapharyngeal soft tissues (See Chap. 11);
- **Zone 4.** Hyoid bone (See Chap. 11), lateral neck soft tissues (See Chap. 11), and oropharynx (See Chap. 13);
- **Zone 5.** Mandibular body.
- **Zone 6.** Maxillary and mandibular dental arches including the dentition and alveolus.

Table 10.1 Differences between reformatted panoramic images from CBCT data and conventional images from classical rotational panoramic radiography

Aspects	Panoramic image type		Clinical significance
	Reformatted	Conventional	
Construction	Layer position and width is most often user defined	Manufacturer defined, with limited modifications (e.g., "v" shaped, normal, broad arch shapes)	CBCT reformatted panoramic image is free from patient positioning errors and artifacts (e.g., "ghost" images)
			CBCT panoramic images can be constructed thin (5–10 mm) or thick (>25 mm) changing visibility of structures
	Custom curved layer to either the maxillary or mandibular dentition	Fixed, usually based on the average shape of the mandibular dentition	As the image layer corresponds to the position of the teeth, there is limited blur of teeth in the dental arch on reformatted panoramic images
	Projection is always perpendicular to the panoramic construction line (spline)	Projection is not perpendicular to the panoramic image layer	There is limited tooth overlap in reformatted panoramic images unlike conventional panoramic images that often show overlap of interproximal contacts, especially in the premolar region
Image layer	Uniform width	Variable width ranging from narrow (10 cm) in the anterior region to wider (25 mm) posteriorly	Anterior teeth, premaxilla and symphyseal region in CBCT reformatted panoramic image are usually in focus
	Structures outside the image layer are excluded from the image	Structures outside the image layer are also included in the image	Soft tissues and airway spaces (appearing as indistinct but characteristic radiopaque shadows superimposed over the osseous and dental structures—e.g., external nose and ear, tongue, airway spaces) and medial and lateral osseous structures (e.g., hyoid bone, zygomatic arch) may not be visualized on CBCT panoramic images
	Undistorted	Wide range of distortion of structures within the image layer not corresponding exactly to the center of the image layer	There is no magnification or distortion of structures, particularly teeth, on reformatted panoramic images

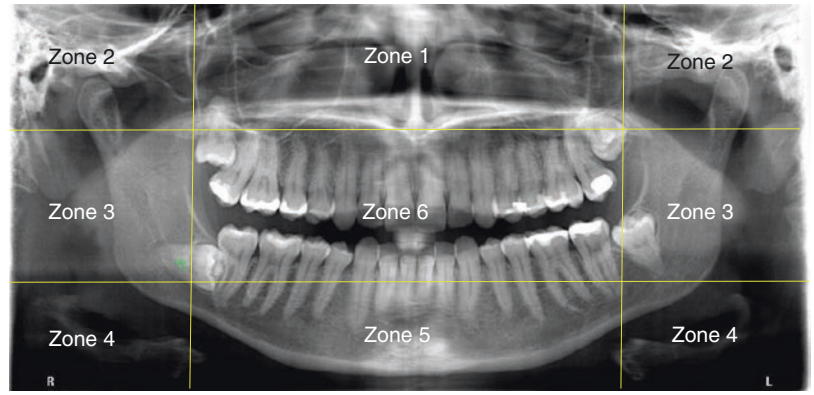

Fig. 10.6 Reformatted CBCT panoramic image demonstrating six regional zones for the assessment of cross-sectional images

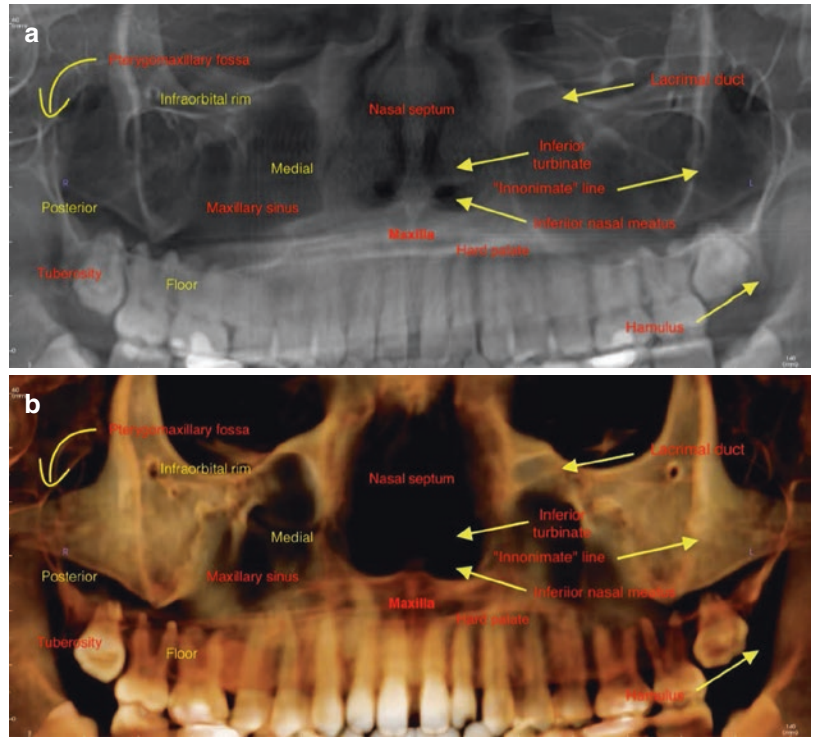

Fig. 10.7 Specific topographic features and anatomic landmarks seen on CBCT reformatted panoramic ray sum (**a**) and volumetric rendered (**b**) images for Zone 1

The utility of the reformatted panoramic image is that it provides a "dentition centric" representation of osseous anatomy of the maxillofacial region incorporating both the maxilla and mandible but also the including aspects of the nasal, sphenoid, zygomatic, and temporal bones (Figs. 10.7, 10.8, 10.9, 10.10, 10.11, and 10.12).

10.2 The Maxilla

The maxilla is an irregularly, pyramid-shaped, bone composed of two symmetrical components (hemi-maxillae) articulated together along the midline of the face with the medial palatine suture or inter-maxillary suture. The medial-superior aspect comprises the nasal

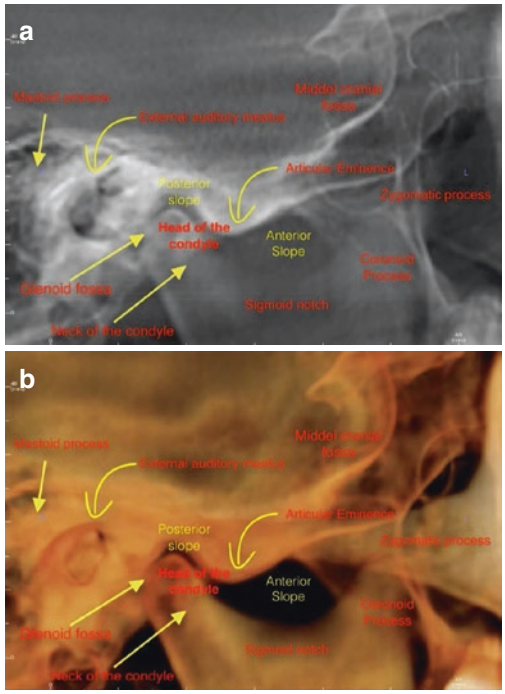

Fig. 10.8 Specific topographic features and anatomic landmarks seen on CBCT reformatted panoramic ray sum (**a**) and volumetric rendered (**b**) images for Zone 2

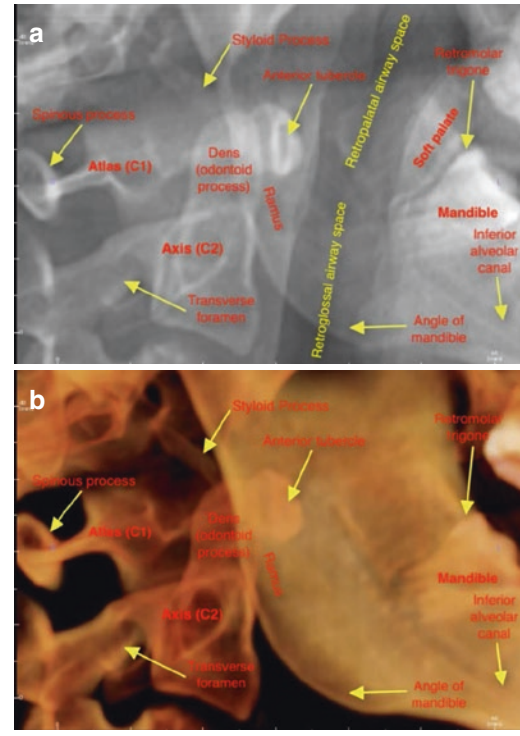

Fig. 10.9 Specific topographic features and anatomic landmarks seen on CBCT reformatted panoramic ray sum (**a**) and volumetric rendered (**b**) images for Zone 3

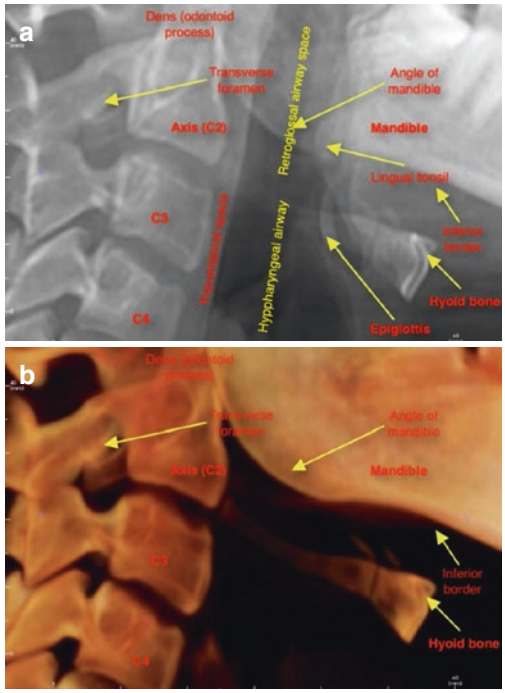

Fig. 10.10 Specific topographic features and anatomic landmarks seen on CBCT reformatted panoramic ray sum (**a**) and volumetric rendered (**b**) images for Zone 4

fossa, folded layers of cortical bone which contain large concavities and expand in all three dimensions, forming a large portion of the midfacial skeleton (Figs. 10.13 and 10.14). More laterally lies the largest component, the body of the maxilla, a "hollowed out" enclosure within which lies the maxillary sinus formed mostly by cortical bone lined by a thin layer of mucosa. The caudal (inferior) aspect of the maxillary bone is the alveolar process, an arch-shaped osseous projection and the palatine process (hard palate), a dome-shaped, concave layer of thick cortical bone which forms the roof of the oral cavity. The alveolar process is composed of cancellous bone lined by a varying thickness of cortical layer and houses the maxillary teeth in thin-walled cortical concavities, the tooth sockets.

Laterally the maxillary body has two zygomatic processes that articulate with the zygomatic bones on either side of the midface and superiorly two frontal processes that articulate

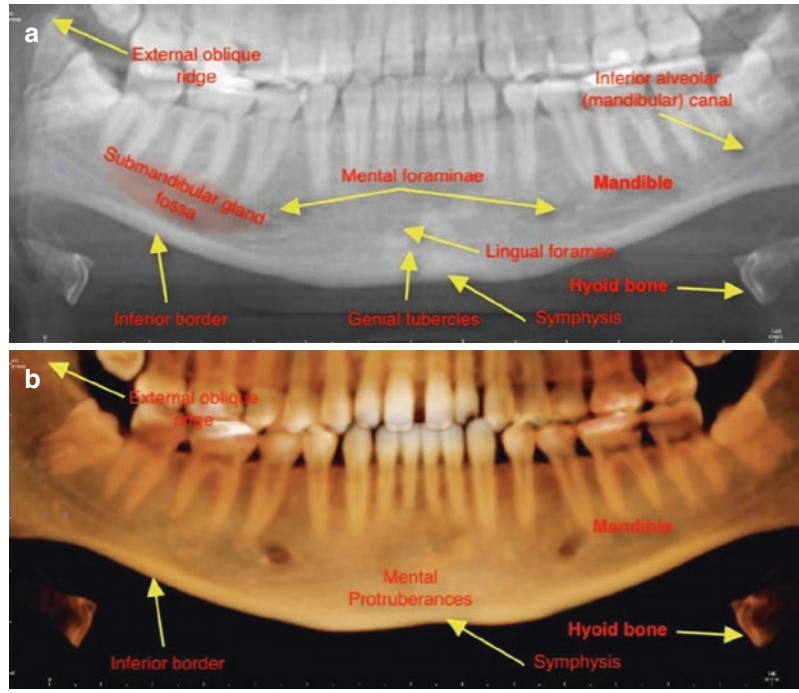

Fig. 10.11 Specific topographic features and anatomic landmarks seen on CBCT reformatted panoramic ray sum (**a**) and volumetric rendered (**b**) images for Zone 5

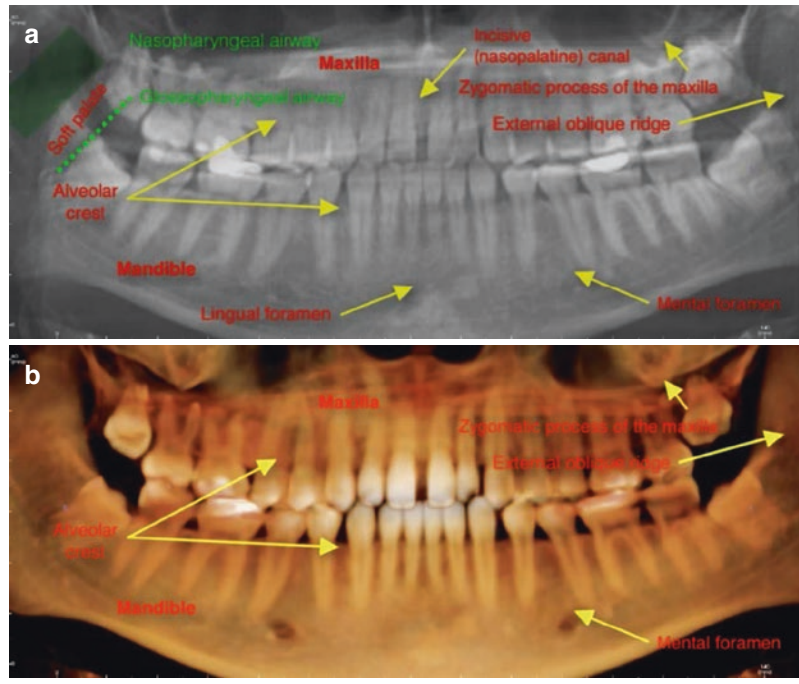

Fig. 10.12 Specific topographic features and anatomic landmarks seen on CBCT reformatted panoramic ray sum (**a**) and volumetric rendered (**b**) images for Zone 6

with the frontal bones and nasal bones. In addition, each hemi-maxilla presents a thick horizontal fold (inferior orbital rim) which extends dorsally forming a horizontal plate (orbital plate of the maxilla) contributing to the formation of the floor of each orbit.

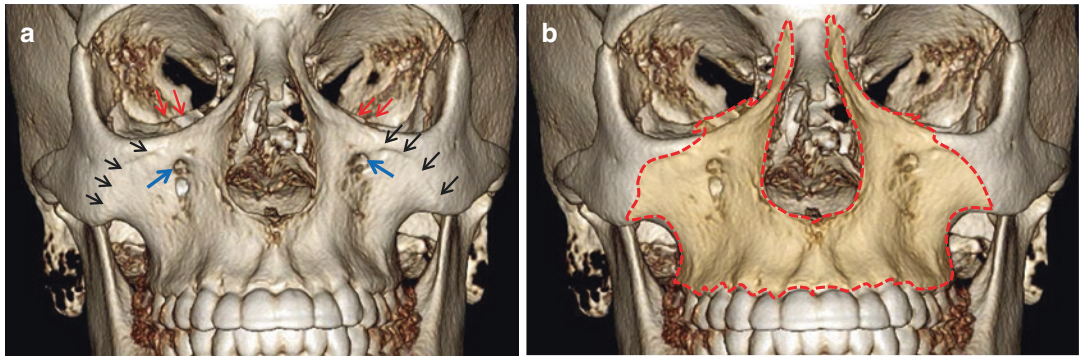

Fig. 10.13 Unmarked (**a**) and annotated (**b**) shaded surface frontal rendering of the midface (facial view) outlining the major components of the maxillary bone: The cephalad thin processes are the frontal processes of the maxilla; the lateral projections of the maxillary bone are the zygomatic processes (*black arrows*); maxillary orbital plates (*red arrows*). The alveolar process is the caudal end of the maxillary bone housing the maxillary teeth. The frontal surface openings are the infraorbital foramina (*blue arrows*)

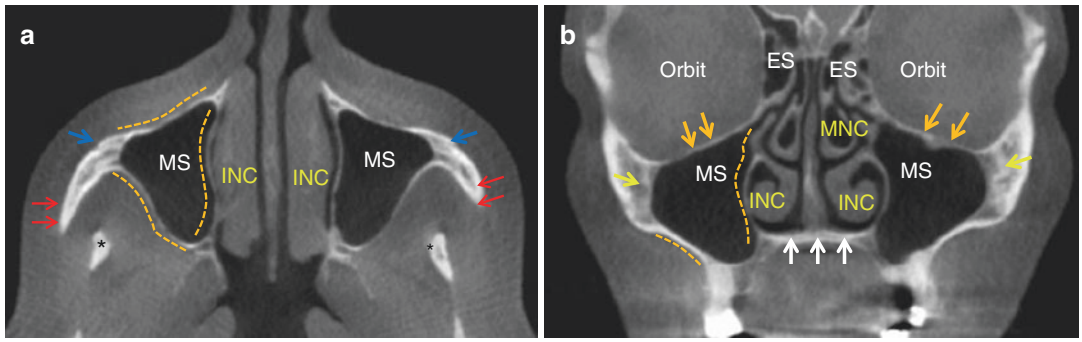

Fig. 10.14 Axial (**a**) and coronal (**b**) orthogonal image outlining the anterior, posterolateral and medial walls of the body of the maxilla (*orange dotted lines* in **a**) lateral and medial walls (**b**) floor of the orbit (*orange arrows* in **b**), zygomatic process of the maxilla (*yellow arrows* in **b**), hard palate (*white arrows* in **b**), zygomatic arch (*red arrows* in **a**), the maxillary sinus (MS), ethmoid sinus (ES), and coronoid process of the mandible (*black asterisk* in **a**)

10.2.1 The Infraorbital Foramen

The infraorbital foramen (IOF) (Figs. 10.15, 10.16, and 10.17) is an important anatomical landmark of the body of the maxillary bone. It is located on the facial aspect of the body of the maxilla approximately 5–6 mm below the inferior orbital rim and just cephalad to the canine fossa, a depression present above the canine, lateral to the ipsilateral nasal cavity. The IOF transmits the infraorbital nerve, a terminal branch of the maxillary nerve (V2), and respective blood vessels. The infraorbital nerve originates inside the pterygopalatine fossa, enters the infraorbital groove (a sulcus on the orbital plate of the maxilla), continues in the infraorbital canal, and exits to the face through the infraorbital foramen. The infraorbital nerve provides sensory innervation to anterior maxillary bone and soft tissue and anastomoses with terminal branches of the posterior superior alveolar nerves.

10.2.2 Posterior Superior Alveolar Canal

Two additional branches of the maxillary neurovascular bundle, the posterior superior alveolar (PSA) and middle superior alveolar (MSA), originate within the pterygopalatine fossa. Both branches travel within the lateral walls of the maxilla and are occasionally visible in either coronal or cross-sectional images of the maxilla

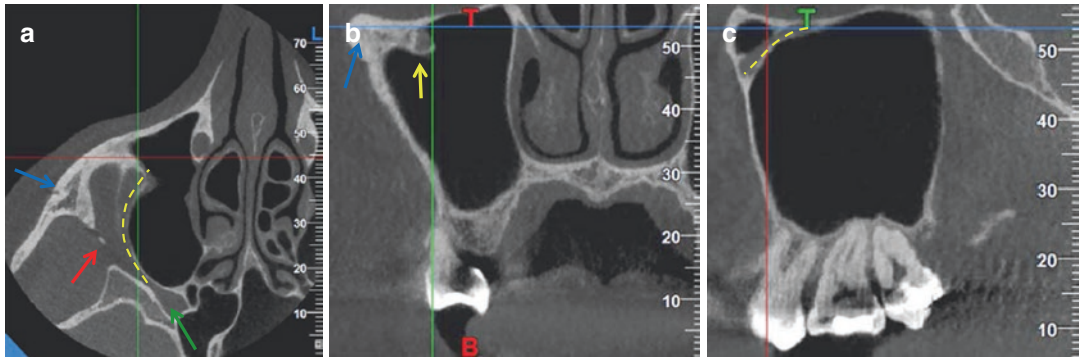

Fig. 10.15 Axial (**a**), coronal (**b**), and sagittal (**c**) orthogonal images depicting the course of the infraorbital nerve inside the orbital plate of the maxillary bone (*yellow dotted line*) from the pterygopalatine fossa (*green arrow*) to its exit point on the facial surface of the body of the maxilla as the infraorbital foramen (*yellow arrow*) (*blue arrow* zygomatic process, *red arrow* inferior orbital fissure)

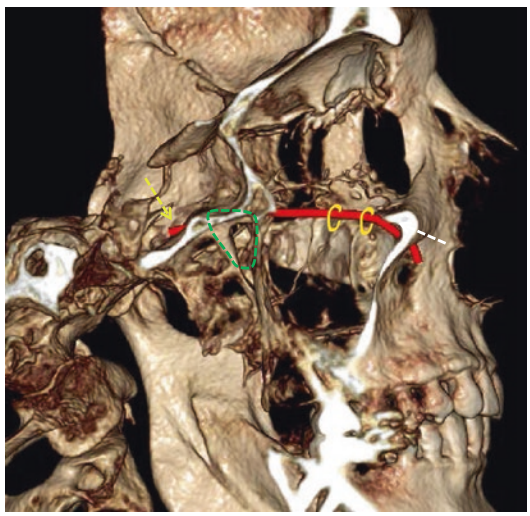

Fig. 10.16 Cropped lateral surface rendering of the midface illustrating the course of the maxillary nerve (V2) from the foramen rotundum (*yellow dashed arrow*) to the pterygopalatine fossa (*dashed green triangle*) where one of the branches, the infraorbital nerve traverses through the infraorbital groove (artistic representation with *orange rings*) to exit through the infraorbital foramen (*white dashed arrow*)

(Fig. 10.18). Both follow an almost horizontal course and appear as small linear hypo-densities at variable distances superior to the alveolar ridge in cross-sectional imaging (de Oliveira et al. 2017). Identification of both the PAS and MSA is important especially in sinus grafting procedures, where bleeding may occur from injury to the PAS artery. This osseous canal may not be visible when its diameter is less than the voxel resolution of the CBCT acquisition.

10.2.3 The Maxillary Alveolar Process

The alveolar process is a horseshoe-shaped, solid osseous inferior extension of the body of the maxilla. It comprises two main parts without obvious physical distinction between the two: the base and the alveolar ridge. The base is the supporting osseous tissue whereas the alveolar process is the tooth-bearing bone. The alveolar process houses the maxillary teeth, the roots of which are usually located within the cortical plates of the alveolar bone. The interproximal surface of the crowns of the teeth aligns in contact forming a continuous dental arch. Tooth position directs and distributes the occlusal forces of mastication to the base of the alveolar bone which is broader in comparison to the crest (Fig. 10.19). With tooth loss, the alveolar bone resorbs and atrophies due to loss of function.

Because the maxillary alveolar ridge is essentially "U" shaped, MPR panoramic reformat and multiple cross-sectional images (perpendicular to the alveolar arch) are the most appropriate images for evaluation (Figs. 10.20 and 10.21). Cross-sectional images of the anterior maxilla demonstrate the shape and size of the respective alveolar ridge around each existing tooth. The facial and

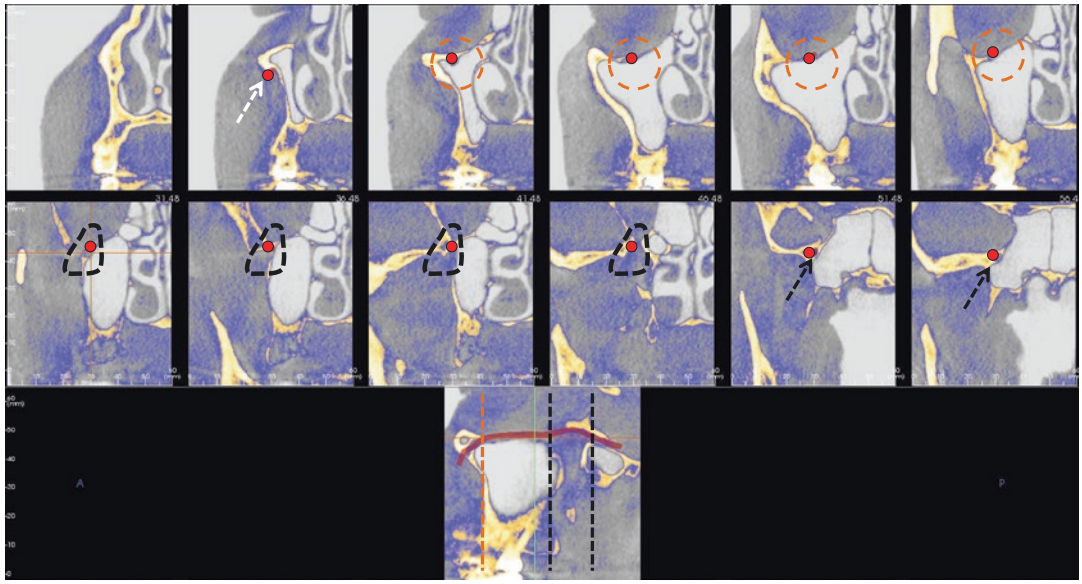

Fig. 10.17 A series of cross-sectional (filters applied) images (*above*) along a custom *curved line* (*below*) which follows the course of the maxillary nerve (V2) and its terminal branch, the infraorbital nerve from the foramen rotundum (*black dashed arrow*) to the pterygopalatine fossa (*black dashed triangle*) to the infraorbital groove (*brown dashed ring*) to its exit through the infraorbital foramen (*white dashed arrow*)

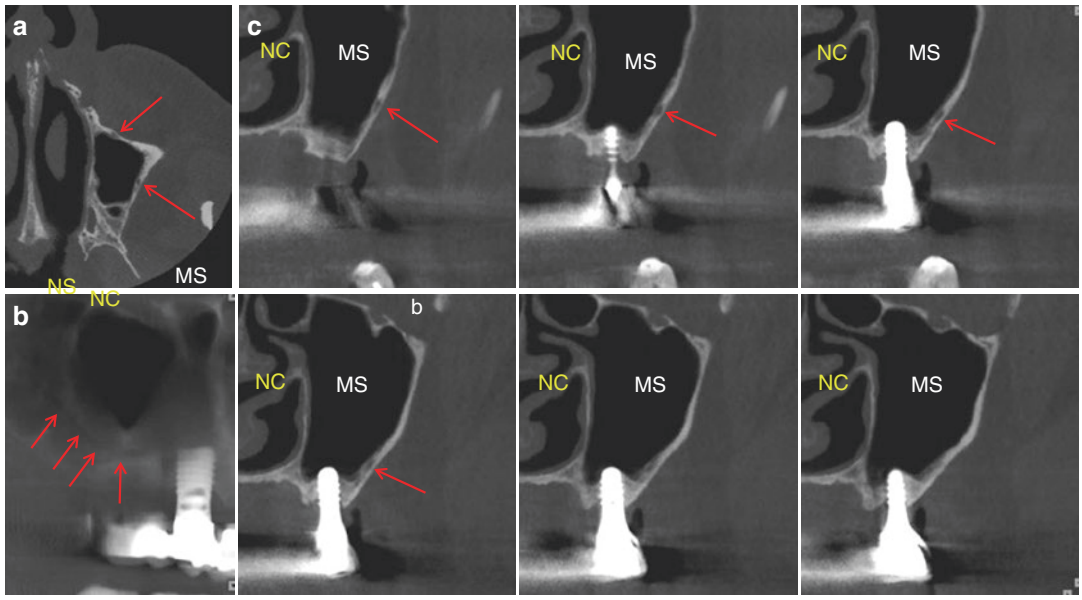

Fig. 10.18 Axial (**a**) and left posterior para-sagittal curved planar thick reformatted (**b**) and a series of cross-sectional images (**c**) show the course of the osseous canal for the PSA neurovascular bundle (*red arrows*) on the lateral wall of the maxillary sinus (MS) (*NC* nasal cavity, *NS* nasal septum)

palatal cortical plates are easily recognized and their integrity and thickness can be assessed. Relevant anatomical limitations of the anterior maxilla are also clearly seen (e.g., the nasopalatine canal). The thickness of the cortical plates adjacent to the roots of the teeth vary and may range from 1 mm or more to imperceivible (Fig. 10.20). Compromised or eroded cortical

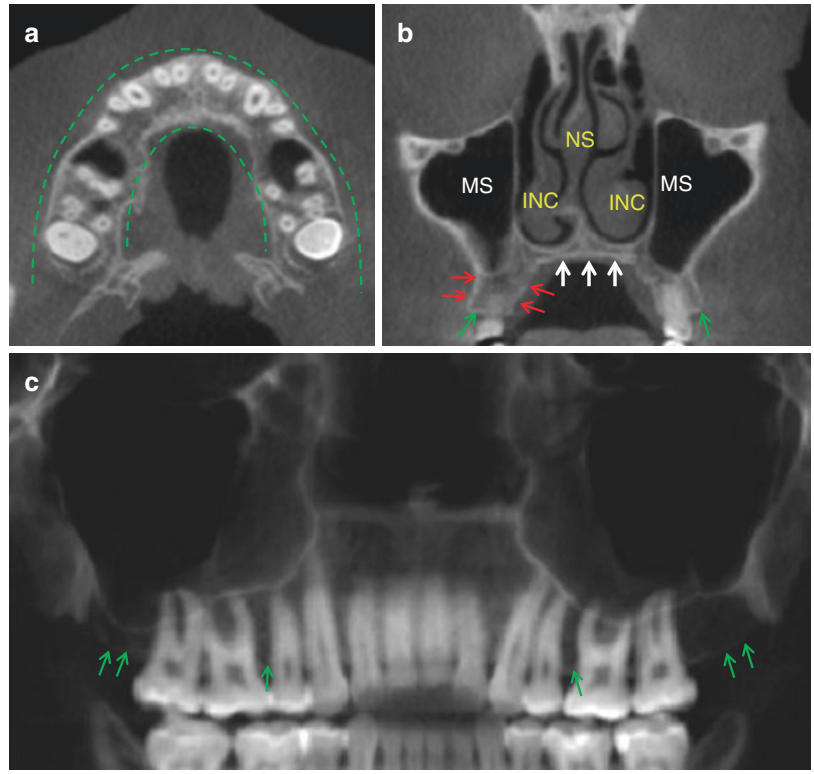

Fig. 10.19 Axial (**a**), coronal (**b**), orthogonal and thick panoramic reformatted (**c**) images of the maxillary alveolar process (*green dotted zone*) showing the existing maxillary teeth and neighboring anatomical structures (*green arrows* alveolar crest, *red arrows* buccal and palatal cortical plates, *white arrows* hard palate, *INC* inferior nasal concha, *MS* maxillary sinus, *NS* nasal septum)

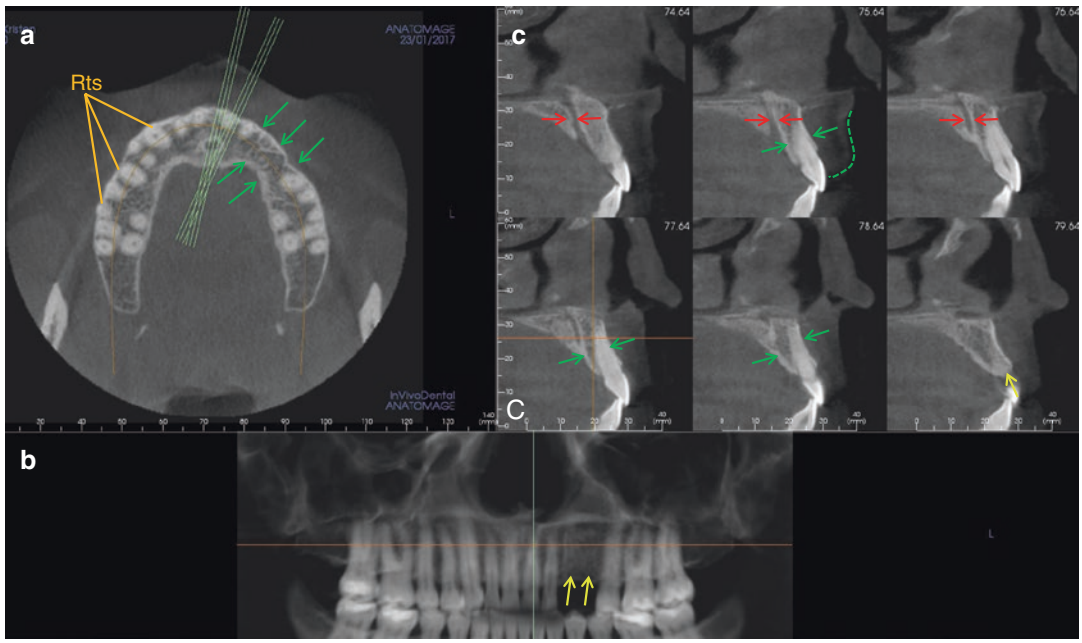

Fig. 10.20 Axial (**a**), thick panoramic reformatted (**b**) and sequential, trans-axial (cross-sectional) (**c**) images of the maxilla illustrating the maxillary alveolar process and regional anatomical structures of the left anterior maxilla (*green arrows* alveolar process, *yellow arrows* alveolar crest, *red arrows* nasopalatine canal, *Rt* roots of the maxillary teeth, *green dotted line* upper lip)

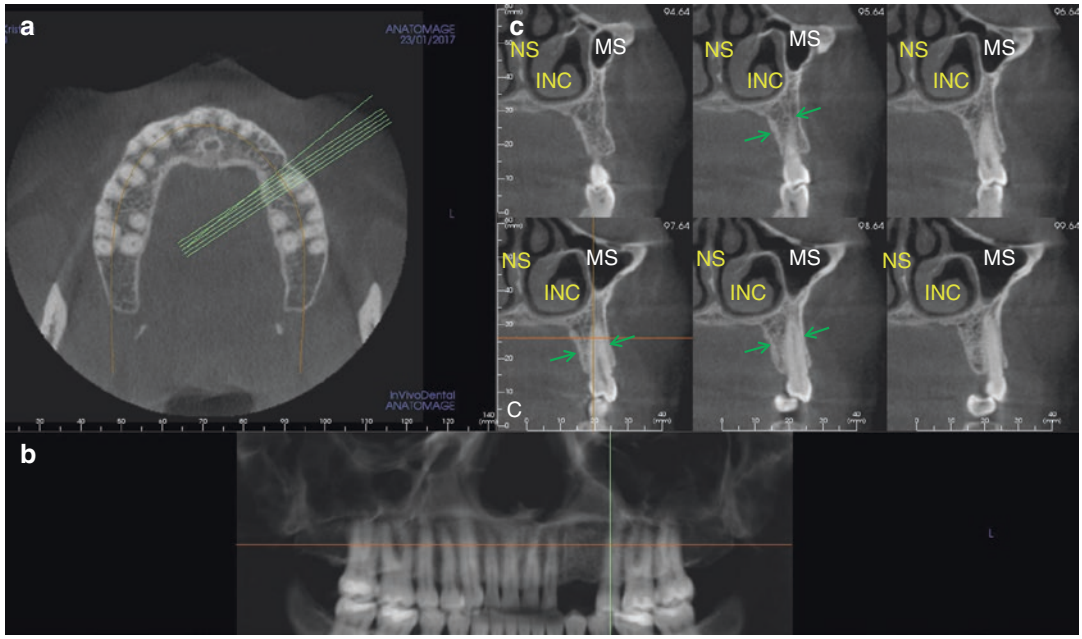

Fig. 10.21 Reference axial (**a**), thick panoramic reformatted (**b**), and sequential, trans-axial (cross-sectional) (**c**) images of the maxilla illustrating the maxillary alveolar process and regional anatomical structures of the left premolar maxilla (*green arrows* cortical plates of the alveolar process, *white arrows* hard palate, *NS* nasal septum, *INC* inferior nasal concha, *MS* maxillary sinus)

plates are often associated with apical pathology in adjacent teeth.

The assessment of the alveolar bone is crucial in edentulous as well as in dentate sites. In edentulous regions, the dimensions of the alveolar bone and its spatial relationship with the opposite alveolar ridge may be shown by sequential cross-sectional images. Moreover, nearby anatomical structures of importance such as the floor of the nasal cavity and floor of the maxillary sinus may be evaluated. Generally the alveolar bone is longer and thinner in the anterior maxilla to accommodate the comparable morphology of the roots of the anterior maxillary teeth.

Sequential cross-sectional images of the posterior maxillary region (Fig. 10.21) show that the alveolar bone gradually reduces in height and increases in width further posteriorly. Lateral portions of the ipsilateral nasal cavity and the entire maxillary sinus are visualized. The maxillary sinus initially appears narrow in the premolar region as this represents the anterior recess. Further posteriorly, the maxillary sinus becomes wider. The relationship of the roots of the premolar teeth to the maxillary sinus floor can be assessed which is important especially if there is developing apical pathology.

In posterior maxillary cross sections the molar teeth and their surrounding alveolar bone are seen (Fig. 10.22). The alveolar process becomes gradually thicker to accommodate the wider roots of the molars and decreases in height to accommodate the maxillary sinus. The thickness of the buccal and palatal cortical plates varies considerably from tooth to tooth. Variation in the root length and peculiarities in the floor of the maxillary sinus may result in an intimate relationship between the two and this should be determined in cases of developing pathology or possible surgical intervention. The maximum width of the maxillary sinus is displayed in this area and images in this region may demonstrate intrinsic or extrinsic sinus disease (see Chap. 30). Cross sections may also depict the PSA neurovascular bundle on the lateral wall of the maxillary sinus (Fig. 10.18).

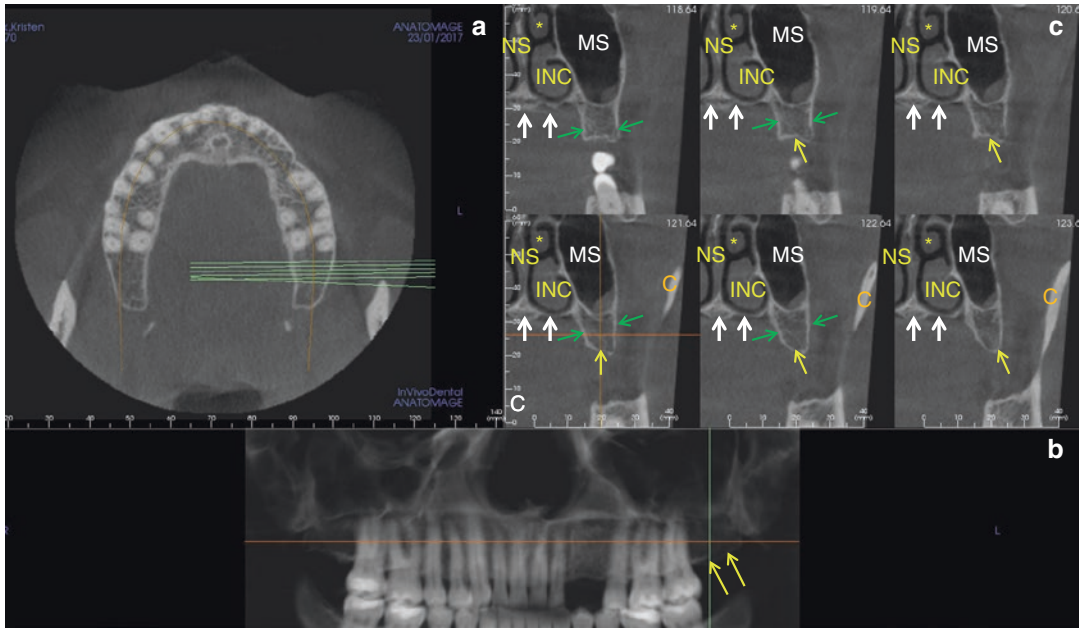

Fig. 10.22 Reference axial (**a**), thick panoramic reformatted (**b**), and sequential, trans-axial (cross-sectional) (**c**) images of the maxilla illustrating the maxillary alveolar process and regional anatomical structures of the left molar alveolar process and relevant neighboring anatomical structures (*green arrows* cortical plates of the alveolar process, *white arrows* hard palate, *NS* nasal septum, *INC* inferior nasal concha, *MS* maxillary sinus, *yellow arrows* alveolar crest, *C* coronoid process of mandible, *NS* nasal septum, *Asterisk* middle nasal concha)

The maxillary alveolar arch terminates at the maxillary tuberosity, a rounded osseous prominence distal to the last molar tooth (third molar). The tuberosity articulates with horizontal plate of the palatine bone and is adjacent to the vertical lateral pterygoid plate of the sphenoid bone. The pterygoid plates of the sphenoid bone may be visualized in the sequential cross sections in the posterior aspect of the maxillary arch if the panoramic spline is extended dorsally (Fig. 10.23). Pending on the height of the reconstructed cross sections, the pterygomaxillary fissure or a portion of it may be visualized (Fig. 10.24). This is a vertically oriented fissure between the posterior wall of the maxillary and the pterygoid process of the sphenoid bone. It connects the infratemporal fossa with the pterygopalatine fossa which serves as a passageway for the PSA neurovascular bundle (a branch of the maxillary nerve-V2) and terminal branches of the maxillary artery.

The alveolar process consists of intramedullary cancellous bone and a peripheral layer of compact, cortical bone, frequently called "the cortical plates." Cross-sectional images of the alveolar bone are best for the assessment of the fine details of bone composition and structure: The thickness of the cortical plates ranges from 1 to 3 mm depending on location, with the palatal cortical plate being thicker than the facial plate (Fig. 10.25). The cancellous bone pattern of the maxilla is usually a fine, delicate trabeculae with a random or occasionally horizontal orientation throughout the alveolar ridge; however, generalized hyperdensity (intramedullary sclerosis) may also present (Fig. 10.26). Trabecular may be sparse in Type 4 bone or in patients with osteoporosis (White and Rudolph 1999; Monje et al. 2015).

10.2.4 The Hard Palate

The hard palate is an elevated, dome-shaped, high density structure that separates the oral cavity from the nasal cavity superiorly. It is formed by the junction of two bilateral horizontal plates. The anterior horizontal plate

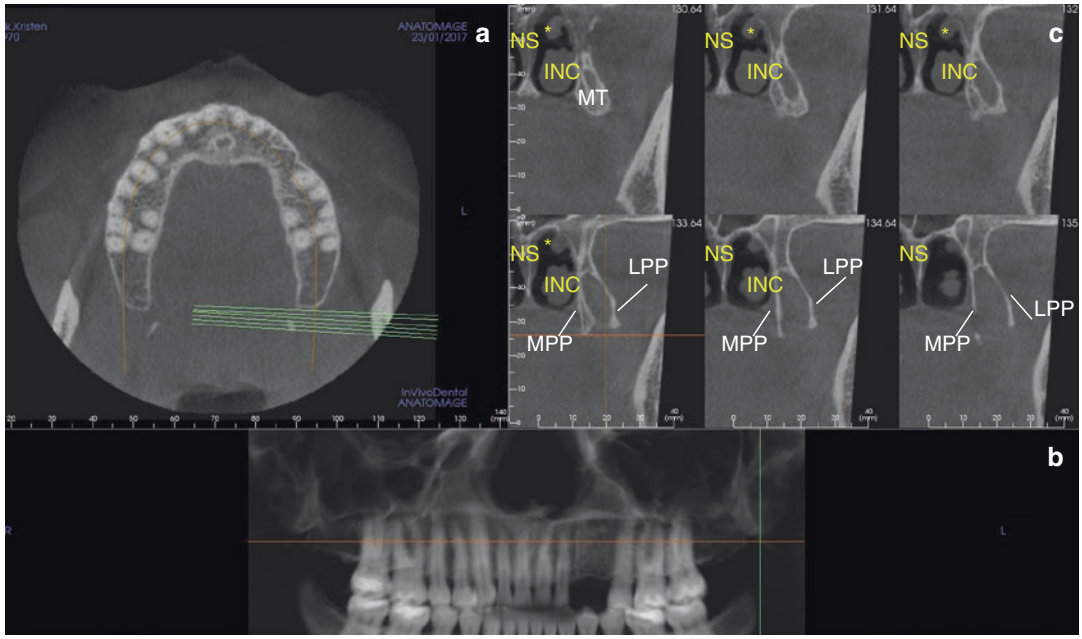

Fig. 10.23 Reference axial (**a**), thick panoramic reformatted (**b**), and sequential, trans-axial (cross-sectional) (**c**) images of the maxilla illustrating the maxillary alveolar process and regional anatomical structures of the left maxillary tuberosity (MT) region and relevant neighboring anatomical structures. (*LPP* lateral pterygoid plate, *MPP* medial pterygoid plate, *MT* maxillary tuberosity, *NS* nasal septum, *INC* Inferior nasal concha, *Asterisk* middle nasal concha)

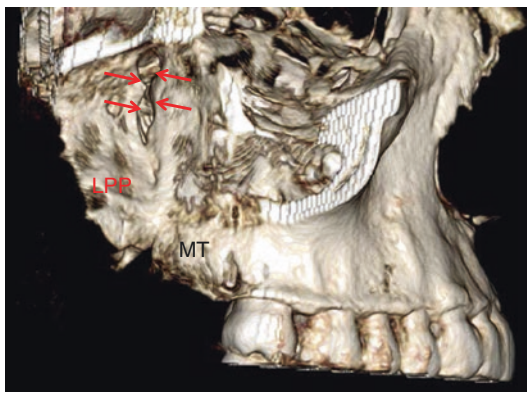

Fig. 10.24 Surface rendering of the right maxilla (lateral view with the zygomatic process segmented) for the assessment of the pterygomaxillary fissure (*red arrows*), the maxillary tuberosity (MT) and the lateral pterygoid process of the sphenoid bone (LPP)

extends medially from the maxillary alveolar process whereas the posterior horizontal plate is the separate palatine bone. The plates articulate in the midline as the medial palatine or the inter-maxillary suture (Fig. 10.27).

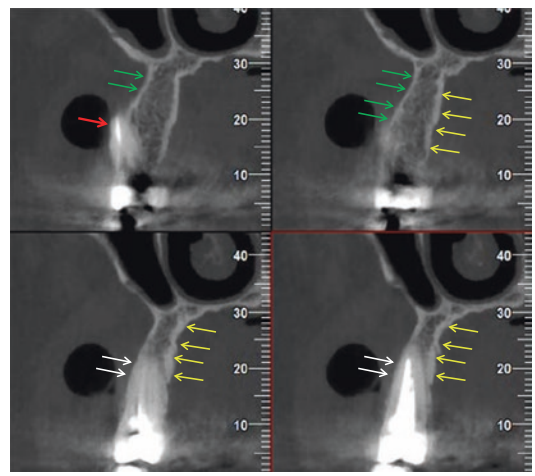

Fig. 10.25 A series of cross-sectional images of the maxillary right second premolar showing the bone architecture of the alveolar process. There is a clear delineation of the buccal (*green arrows*) and palatal (*yellow arrows*) cortical plates. The homogenous fine trabecular pattern of the cancellous bone is characteristic of the maxillary alveolus. Note the minimal buccal cortical coverage of the root of the root canal filled tooth (*white arrows*) and the fenestration of the mesio-buccal root of the adjacent first maxillary molar through the buccal alveolar plate

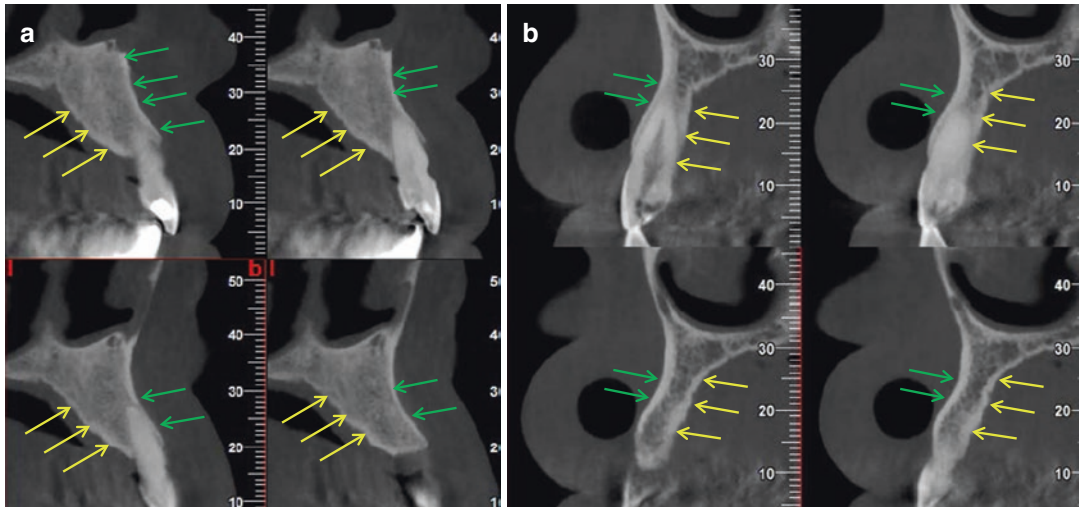

Fig. 10.26 Sequential cross-sectional images of the anterior maxilla in a patient with dense homogeneous trabeculation (**a**) and sparse fine trabecular pattern (**b**). The arrows show the buccal (*green arrows*) and palatal (*yellow arrows*) cortical plates in the respective alveolar processes

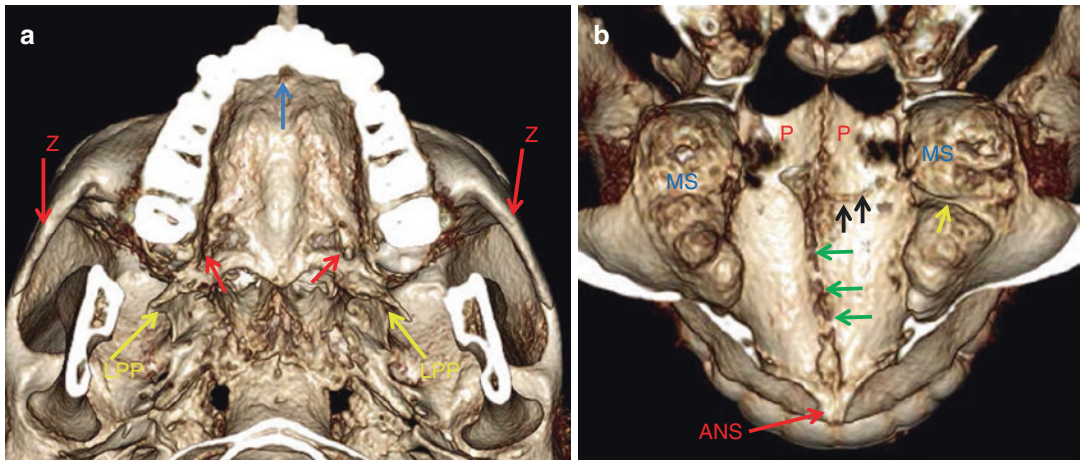

Fig. 10.27 Inferior (**a**) and superior (**b**) surface rendering projections of the hard palate and skull base (partially) showing the hard palate of the maxillary bone and relationship to the alveolar process (*LPP* lateral pterygoid plate, *Z* zygomatic arch, *MS* maxillary sinus floor, *P* palatine bone, *ANS* anterior nasal spine, *red arrow* greater palatine foramen, *blue arrow* incisive foramen, *green arrows* inter-maxillary suture, *black arrows* transverse palatine suture (junction of the maxillary bone and palatine bone), *yellow arrow* septum in maxillary sinus)

Important anatomical landmarks of the hard palate include the nasopalatine canal in the anterior hard palate and the greater and lesser palatine foramina in the posterior hard palate.

10.2.4.1 Nasopalatine Canal

The nasopalatine canal and its inferior opening, the incisive foramen are seen in the midline of the maxillary bone. The nasopalatine canal has its origin on the floor of the nasal cavity where it starts with two separate openings (Fig. 10.28), the superior foramina or foraminae of Scarpa. It continues in a caudal direction towards the palatal aspect of the maxillary bone and runs almost parallel to the labial cortical plate, as seen in the midline cross sections of the maxilla (Fernandez-Alonso et al. 2015). It terminates as the incisive foramen which is located just deep to the palatal papilla between the central incisors. The canal carries

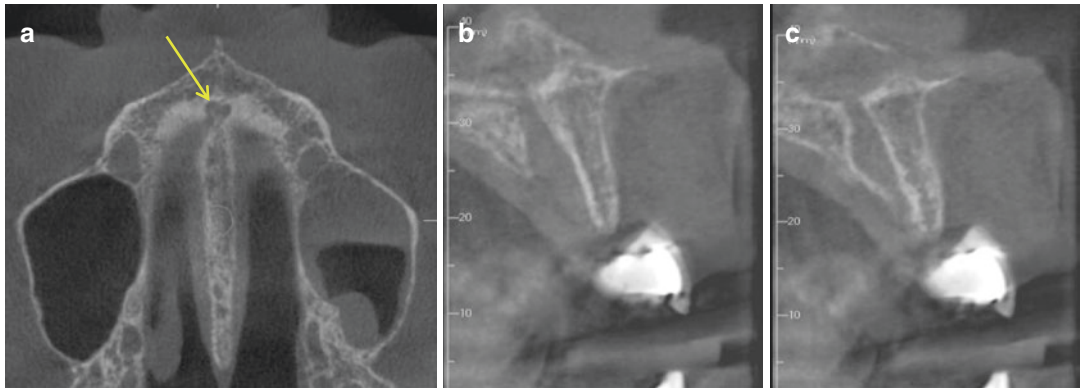

Fig. 10.28 Axial (**a**) and sequential cross-sectional images (**b**, **c**) of the nasopalatine canal. Two small foraminae are identified on the floor of the nasal cavity (*yellow arrow*) as the superior origin of the nasopalatine canal

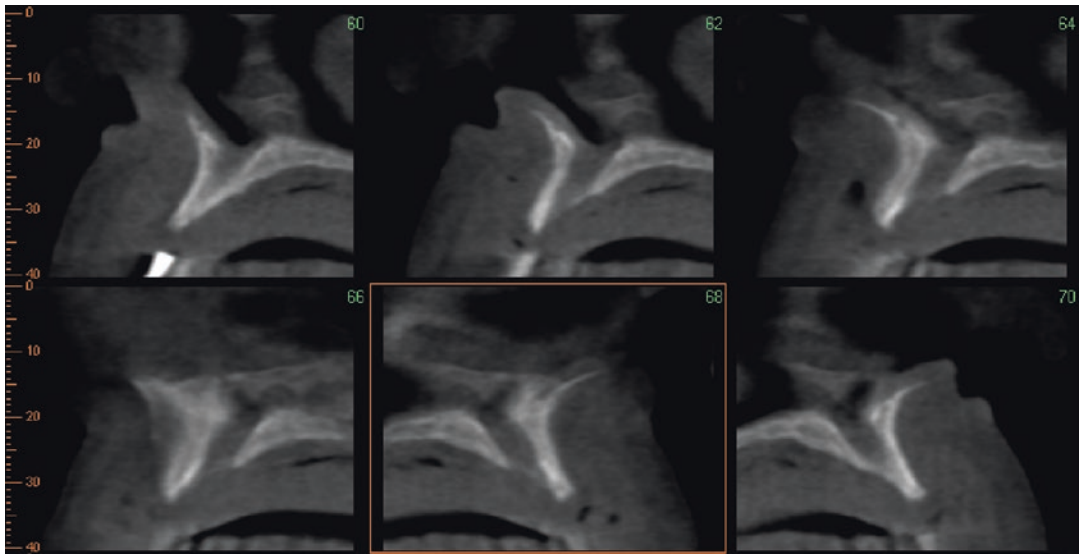

Fig. 10.29 Sequential cross-sectional images of an anterior edentulous maxilla depicting the nasopalatine canal. The canal appears to be considerably widened, reducing the width of the available residual alveolar ridge in the central incisor area

the nasopalatine nerve which supplies sensory innervation to the anterior hard palate. The diameter of the nasopalatine canal may vary, and due to its location, it may compromise the width of the maxillary alveolar bone close to the midline (Fig. 10.29).

10.2.4.2 Greater and Lesser Palatine Canals

The greater palatine foramen is located in the horizontal part of the palatine bone, on either side of the hard palate at the junction of the alveolus and opens medial to the second molar tooth, approximately 10 mm or less from the palatal alveolar crest (Figs. 10.30 and 10.31). It is the terminal end of the greater palatine canal, an osseous canal that connects the pterygopalatine fossa to the oral cavity. The canal contains the greater palatine nerve and respective blood vessels which exit the foramen and spread along the ipsilateral hard palate (Hafeez et al. 2015).

The lesser palatine foramen is located slightly posterior to the greater palatine one, is smaller in diameter, and contains the lesser palatine nerve and blood vessels (Fig. 10.30).

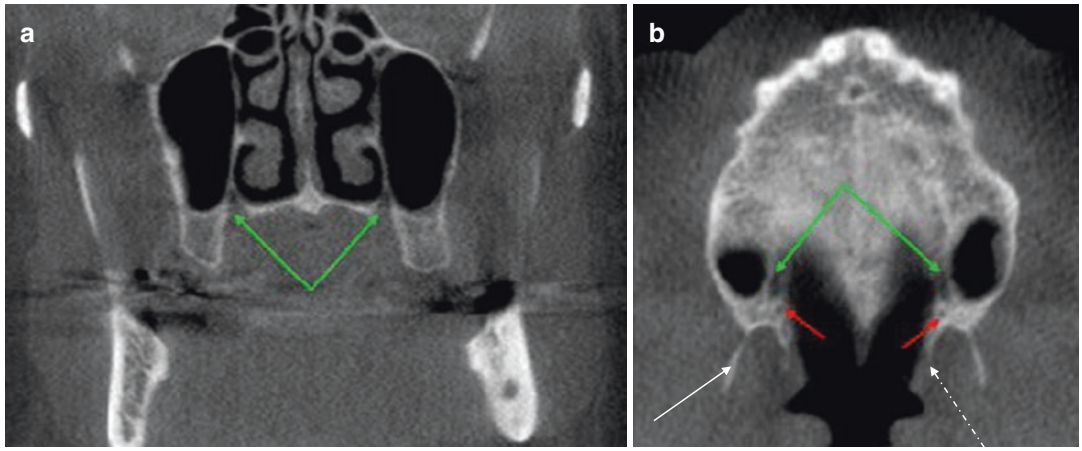

Fig. 10.30 Coronal (**a**) image through the posterior maxilla and axial image (**b**) at the level of the maxillary arch. The *green arrows* identify the greater palatine foramina at the junction of the hard palate and the palatal aspect of the alveolar ridges towards the posterior end of the maxillary arch. The *red arrows* show the lesser palatine foramina. The lateral (*solid white arrow*) and medial (*dashed white arrow*) pterygoid plates are also shown

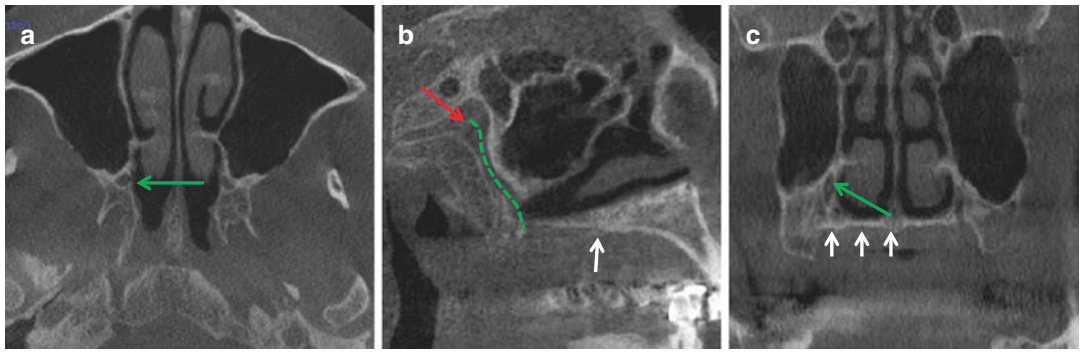

Fig. 10.31 Axial (**a**) corrected sagittal (**b**) and coronal (**c**) CBCT images of the hard palate tracking the course of the greater palatine canal (*green dashed line*) from the pterygopalatine fossa (*red arrow*) to the greater palatine foramen (*green arrow*) (*white arrows* hard palates)

10.3 The Mandible

The mandible is the largest bone of the facial skeleton and lies caudally (below), and articulates with, the maxilla. It forms the lower third of the face. It is "U" shaped bone with a thick outer layer of cortical bone. It is formed from the fusion of the two hemi-mandibles along a vertical line in the midline of the anterior mandibular symphysis. The mandible comprises the mandibular body and the posterior rami, two flattened, vertical projections that articulate with the temporal bone via the mandibular condyle. The mandibular alveolar process contains the teeth and lies integrated superiorly with the basal bone of the body of the mandible.

Each ramus ends in two individual osseous processes: the coronoid process (ventrally), a thin, triangular, and sharp process which serves for muscle attachment and the condylar process (dorsally), an ovoid structure which is articulated with the temporal bone to form the temporomandibular joint (TMJ) (Fig. 10.32).

10.3.1 Mandibular Body

The body of the mandible is composed of two indistinguishable parts: the tooth-bearing alveolar process and the base or basal bone of the mandible which serves as the tooth supporting part.

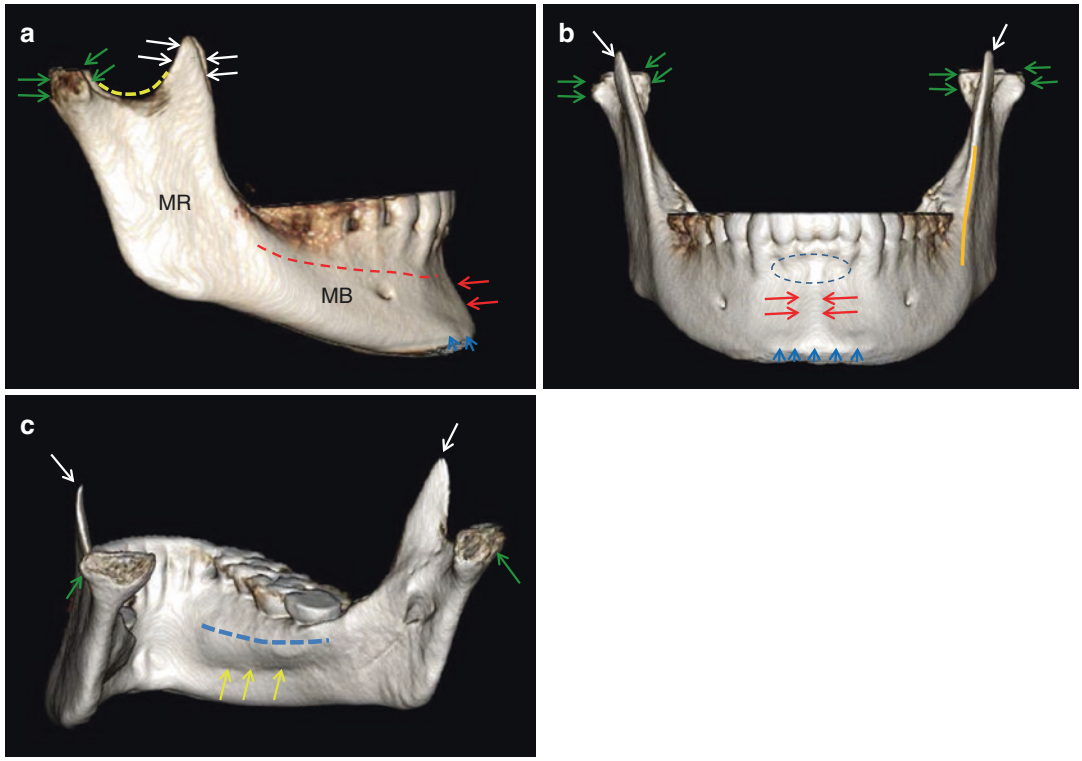

Fig. 10.32 Right lateral (**a**), frontal (**b**), and right lateral posterior (**c**) projections of a shaded surface rendering of the mandible showing anatomical landmarks and topographic features of the mandible (*MR* mandibular ramus, *MB* mandibular body, *green arrows* condylar process, *white arrows* coronoid process, *red arrows* mandibular symphysis, *yellow arrows* submandibular fossa, *blue arrows* mental ridge, *yellow dotted line* alveolar process, *orange line* external oblique ridge, *blue dotted line* internal oblique ridge, *dotted oval* mental fossa)

Severe atrophy may occur of the alveolar process with long-term edentulism leaving the residual basal bone.

A sequence of reformatted panoramic and serial trans-axial (cross-sectional) images are the most appropriate to assess the mandibular bone. These projections will demonstrate the composition of the mandibular bone, the spatial orientation of the alveolar ridge in relation to the opposing dentition and important anatomical structures in the region under examination.

The mandibular bone is surrounded by a thick cortex, thicker than that of the maxillary bone. While there is wide variation, the lingual cortex is often thicker than the labial. The thickest cortical bone is usually the inferior cortex whereas the thinnest cortical plates are in the anterior mandible.

The intramedullary cancellous bone of the mandible differs from that of the maxilla in that the trabeculae are more sparse, longer, sharper, and demonstrate a clear horizontal orientation (Figs. 10.33, 10.34, and 10.35). There is great variability in trabecular pattern related to numerous factors such as location, age, hormonal factors, and degree of edentulism.

10.3.1.1 Anterior Mandible

Sequential cross-sectional images of the anterior mandible demonstrate the orientation of the mandibular bone and anterior teeth in regard to the sagittal plane (Fig. 10.36). The mandibular bone shows a slight labial inclination in cross section that may be more prominent in some individuals. This may result in a prominent concavity, the mental fossa, which is bordered caudally by the mandibular symphysis, a vertical protuberance formed by the junction of the two hemi-mandibles along the midline. The mental

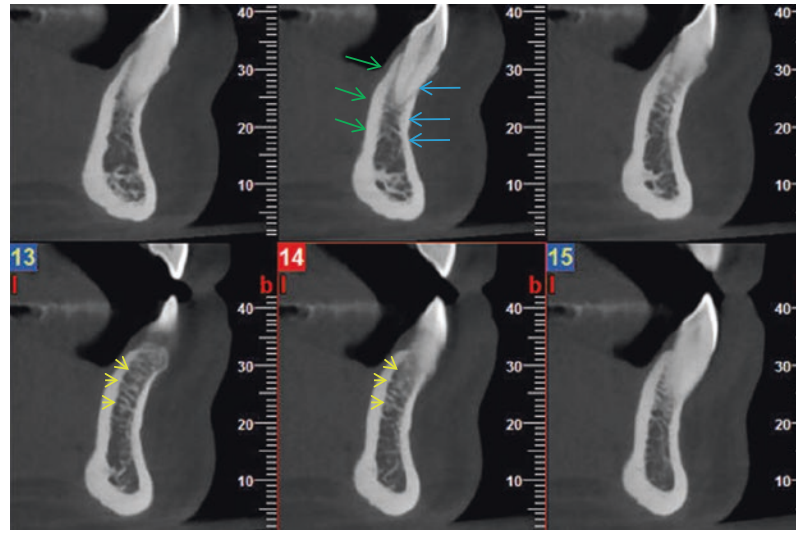

Fig. 10.33 Sequential 1 mm interval transaxial images of the anterior mandible showing the labial (*blue arrows*) and lingual (*green arrows*) cortical plates as well as the trabecular pattern of the cancellous bone in the anterior mandible. Note the elongated, horizontally oriented trabeculae which become more sparse towards the base of the mandibular bone

ridge is a horizontal projection of the labial mandibular cortex which blends to the inferior cortex and forms the chin (Fig. 10.37). The mandibular bone is thinner superiorly towards the alveolar process and becomes considerably thicker and denser inferiorly.

In the edentulous anterior mandible, the alveolar bone varies considerably in height and width. Deviation between the long axis of the alveolar bone and that of the previous anterior teeth is not unusual. In addition, presence of labial and/or lingual undercuts may alter the shape of the alveolar bone dramatically and may render specific locations non-restorable with dental implants (Fig. 10.38).

Additional anatomical structures of importance visualized in the cross-sectional images of the anterior mandible include:

- **The genial tubercles**. The genial tubercle is a projection of the lingual mandibular cortex towards the inferior half of the mandibular bone. It is a high density area, frequently irregular in shape which serves as an attachment point for a number of muscles of the tongue as well as suprahyoid neck (Fig. 10.39).
- **Lingual foramen.** The lingual foramen (also reported as the median, middle, or central lingual foramen) is a vascular canal carrying the terminal branches of the sublingual artery located either on or in close proximity to the genial tubercles in the midline in up to 80% of individuals (Tepper et al. 2001). Smaller "inferior midline foramina" have also been reported, inferior to the genial tubercle(s) in up to 76% of individuals (Figs. 10.39 and 10.40) (Shiller and Wiswell 1954).
- **Accessory Lingual Foramina.** Lateral accessory lingual foramina have been detected between the regions of lateral incisors and the mandibular premolars, towards the inferior border of the mandible (Chapnick 1980) (Fig. 10.41).
- Some blood vessels associated with these accessory foramina may be of sufficient size to be implicated in severe hemorrhaging if injured during implant placement in the mandibular anterior region (Kalpidis and Setayesh 2004). Despite the fact that these vascular channels are identified fairly low on the lingual aspect of the mandibular bone (towards the inferior third of the mandibular bone height), their relative position in relationship to the crest of the alveolar bone may change if bone atrophy is present in the anterior mandible (Fig. 10.41). As a result they may pose as important anatomical limitations in implant surgery if considerable bone atrophy is noted.

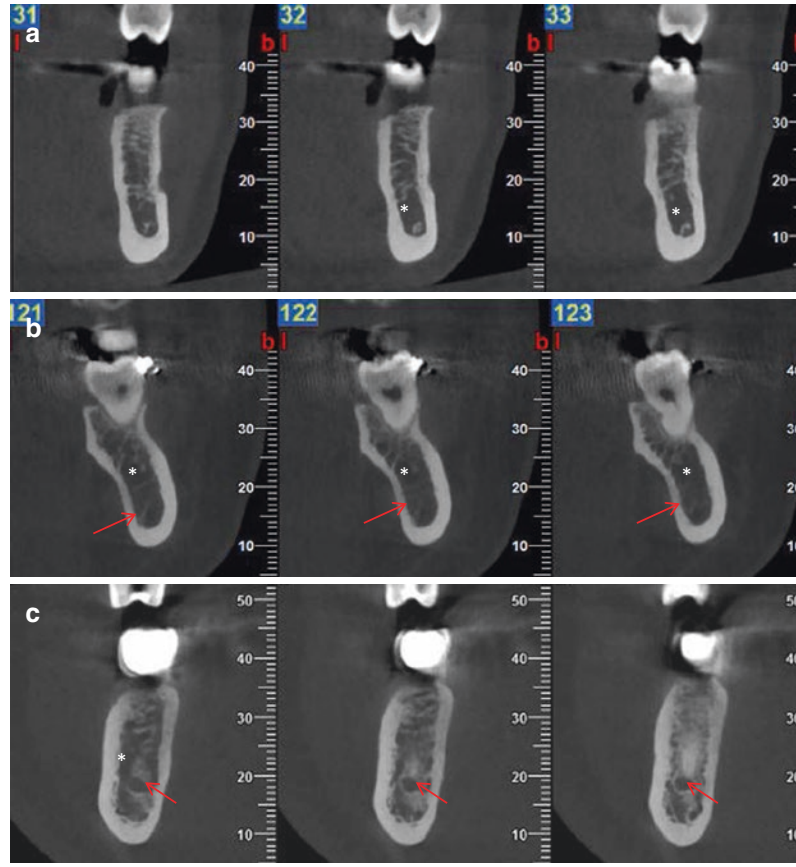

Fig. 10.34 Sequential, 1 mm interval, trans-axial images of the left posterior mandible at the level of the premolar and mental foramen (**a**) and molar (**b**) regions depicting gradual changes in the trabecular pattern. Note the long and narrow horizontal trabeculae which become more sparse within the basal bone and multiple voids (*Asterisk*). Trans-axial images of the same individual in the region of the right molar (**c**) showing a different trabecular pattern associated with the mandibular canal (*red arrows*)

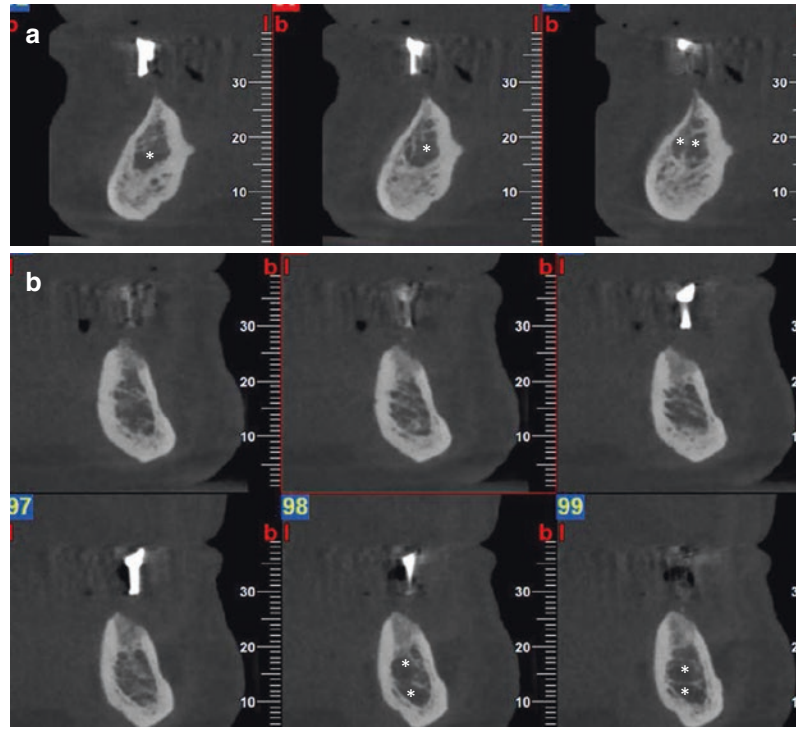

Fig. 10.35 Sequential trans-axial images of the right (**a**) and left anterior (**b**, **c**) edentulous mandible showing the variability in the trabecular pattern from site to site in the same individual. Note that the *horizontal* orientation of the trabeculae and sporadic presence of voids (*Asterisk*) in the mandibular bone

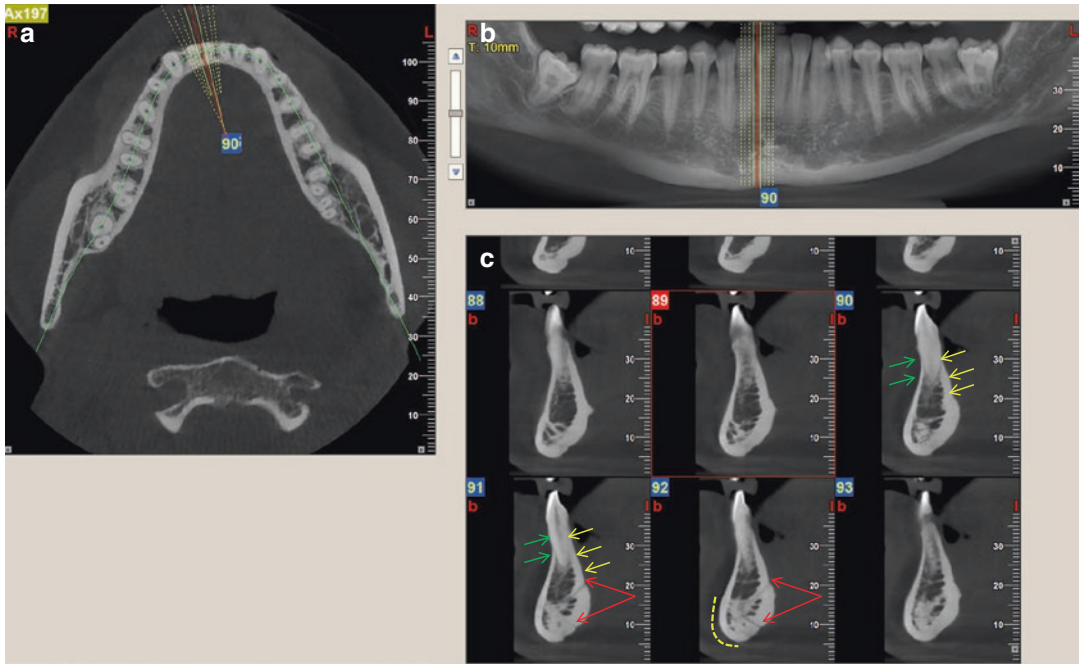

Fig. 10.36 Axial (**a**), reformatted panoramic (**b**), and serial cross-sectional (**c**) CBCT images of the mandible illustrating the mandibular alveolar process and relevant neighboring anatomical structures in the left anterior region. Cross-sectional images (**c**) are optimal in showing the alveolar bone height and width, labial (*green arrows*) and lingual (*yellow arrows*) cortices, the mental ridge (*yellow dotted line*) and the lingual foraminae (*red arrows*)

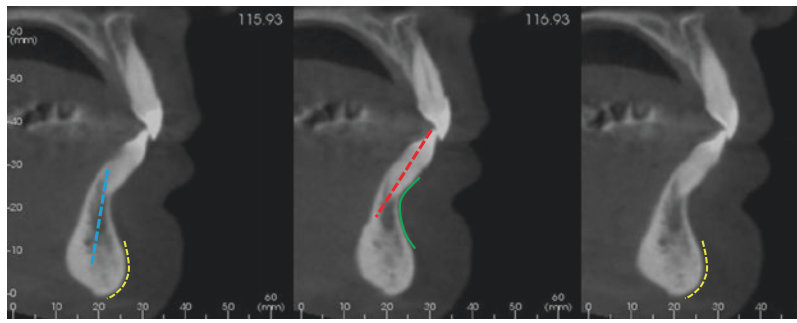

Fig. 10.37 Sequential 1 mm interval trans-axial images of the anterior mandible (central incisor region) demonstrating a marked labial inclination of the mandibular incisors (*red dotted line*) in relation to the more perpendicular orientation of the alveolar bone (*blue dotted line*). This discrepancy accentuates the anatomical concavity, mental fossa (*green curved line*) just below the alveolar crest (*yellow curved dotted line*, mental ridge)

10.3.1.2 Posterior Mandible

In posterior mandibular cross sections (Fig. 10.42, 10.43, and 10.44), the most important topographic anatomical structures include:

- **The external oblique ridge.** This is a fairly smooth ridge present on the buccal aspect of the mandibular bone (originating in the molar region) and extends posteriorly where it ends as the continuation of the anterior border of the mandibular ramus. This line serves as the linear bony attachment of the buccinator muscle) (Fig. 10.43 and 10.45).
- **The internal oblique ridge or mylohyoid line.** The mylohyoid muscle originates from the mylohyoid line (internal oblique ridge) and

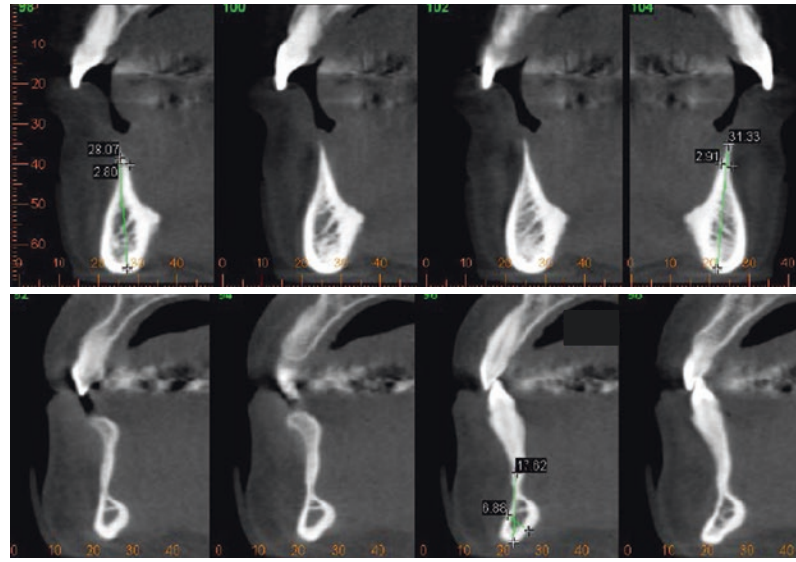

Fig. 10.38 Sequential trans-axial images at 1 mm intervals of the anterior edentulous mandibular region showing "knife-edged" appearance of the alveolar crest and severe horizontal atrophy of the alveolar bone resulting in thinning. Even the width of the tooth-bearing area is markedly reduced

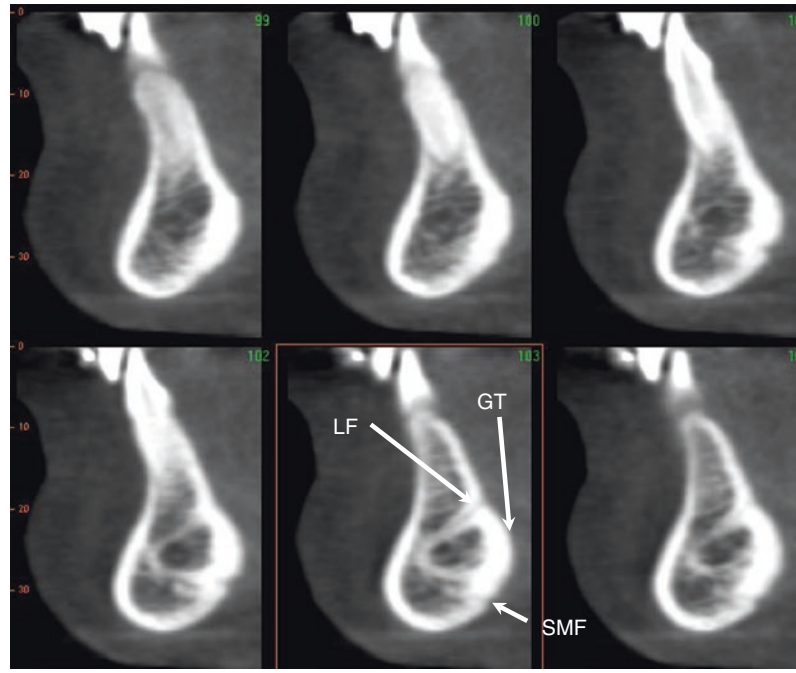

Fig. 10.39 Sequential 1 mm interval trans-axial images of the mandibular anterior midline demonstrating the genial tubercle (*GT*) and the lingual foramen (*LF*) or median lingual foramen. Additional midline foramina are not uncommon in the region. This includes the submental foramina (*SMF*) which contains an artery at the mid-symphysis and anastomoses with the incisive canal. These foramina/canals carry nutrient blood vessels, and may cause severe bleeding if they are perforated during implant surgery

continues in a downward direction towards the hyoid bone where it inserts (Fig. 10.42) This muscle is the biggest contributor to the formation of the floor of the mouth and its presence limits the detection of significant mandibular lingual undercuts. In addition, considerable variation exists as far as it determines the depth of the submandibular gland fossa.

- **The submandibular gland fossa (depression).** This is an anatomical concavity towards the lower half of the mandibular bone in the molar region which nests, partially, the submandibular salivary gland. This may pose an anatomical limitation in implant placement in the region due to the fact that important significant anatomical structures such as the lingual artery are located in the vicinity of the lingual mandibular cortex (Figs. 10.43 and 10.44). The mandibular canal is frequently seen as a well-defined, round or ovoid, small, low density area towards the inferior third of the alveolar bone.

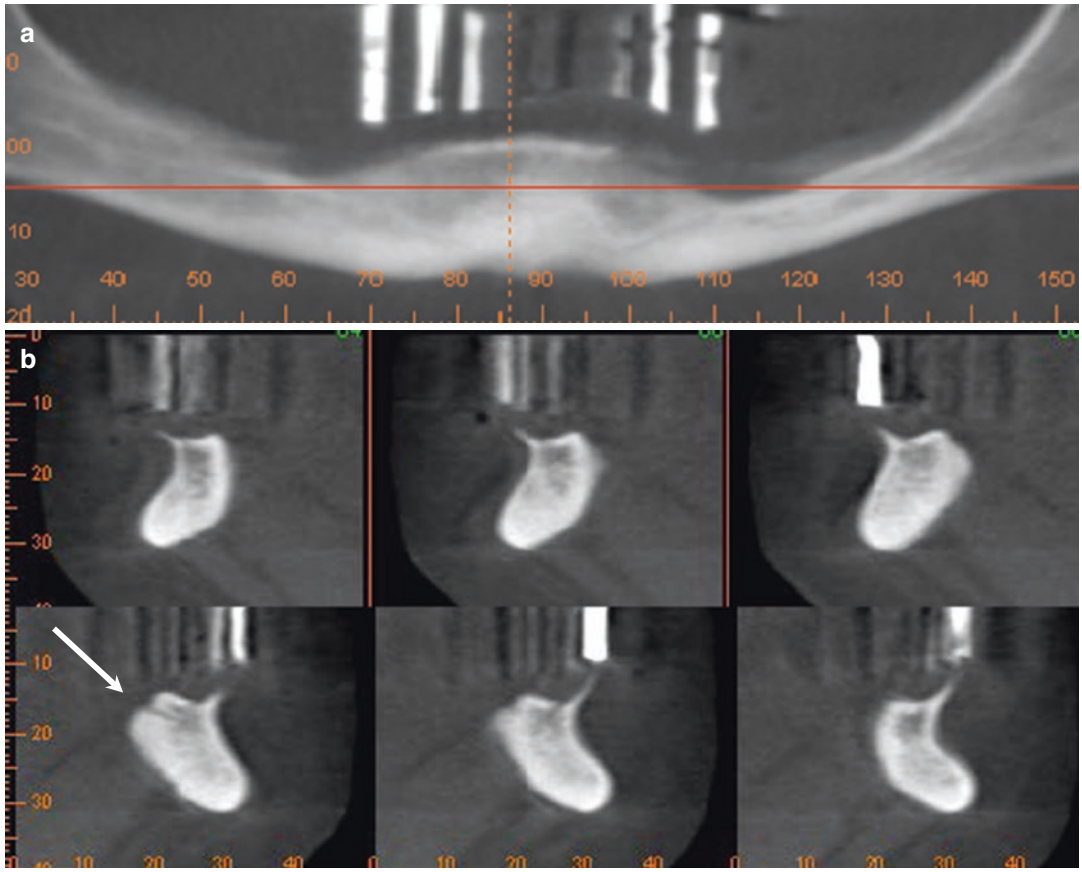

Fig. 10.40 Panoramic (**a**) and sequential trans-axial (**b**) images of the anterior region in a severely atrophic mandible. The cross-sectional images demonstrate an almost "knife-edged" crest and severe lingual inclination of the alveolar ridge. The lingual foramen (*arrow*) appears to be very close to the crest, in a site planned for implant placement (see opaque marker above the alveolar crest). The relative position of the lingual foramen has changed due to the severe atrophy

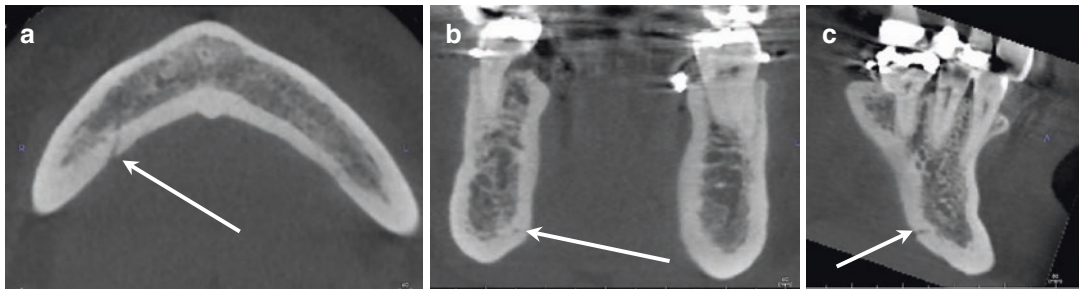

Fig. 10.41 Axial (**a**), coronal (**b**), and sagittal (**c**) CBCT images showing the location of sublingual foraminae (*arrow*) Accessory foramina, like the one demonstrated, have a reported incidence of approximately 65%

It is well known that the loss of teeth will result in a gradual atrophy of the alveolar bone in height and width (Fig. 10.44). As the edentulous bone becomes more atrophic, the relative position of crucial (for surgery) anatomical structures may become more important (Fig. 10.45). Moreover, the pattern of bone resorption (especially in the bucco-lingual aspect) in combination with the possible lingual undercuts mentioned earlier may alter considerably the angulation of

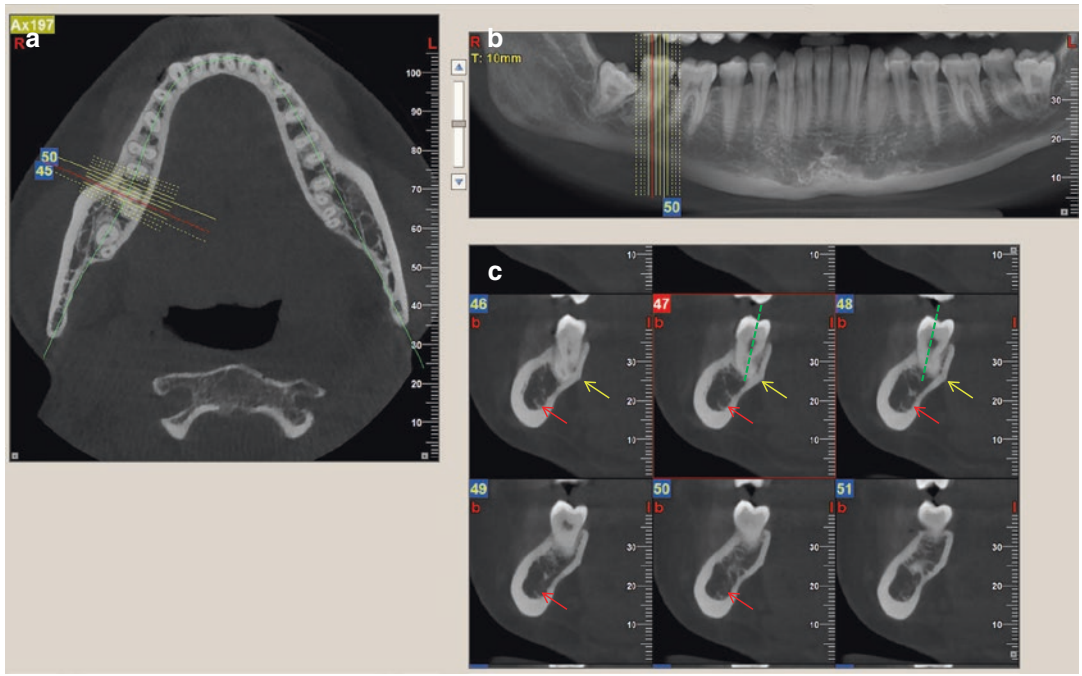

Fig. 10.42 Axial (**a**), reformatted panoramic (**b**), and serial cross-sectional (**c**) CBCT images of the right mandibular molar region illustrating the mandibular alveolar process and relevant neighboring anatomical structures. These images optimally depict the alveolar bone height and width, internal oblique ridge (*yellow arrows*) and the mandibular canal (*red arrows*). Note long axis of the molars (*green dotted line*) in comparison to that of the mandibular bone

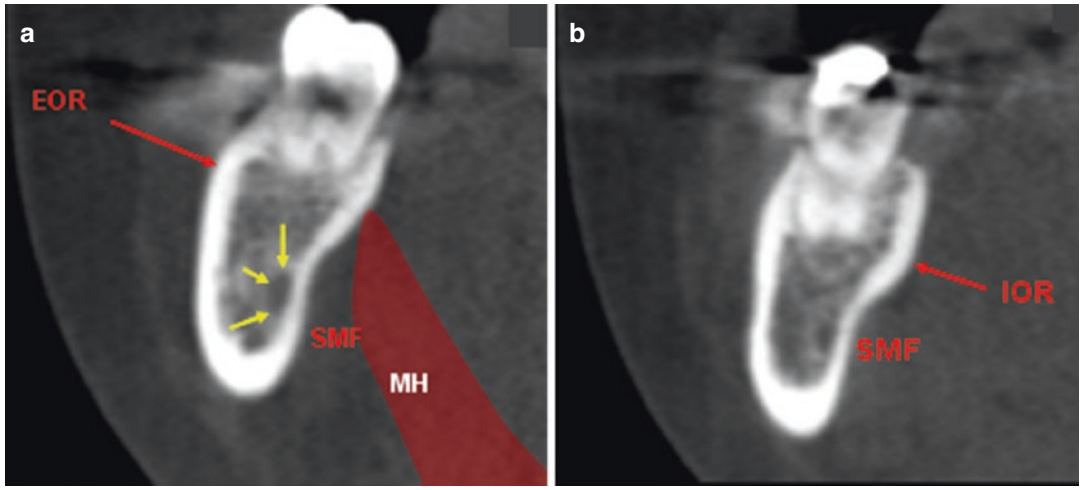

Fig. 10.43 Consecutive cross-sectional images (**a**, **b**) of the right posterior mandible. The superimposed schematic annotates the approximate origin of the mylohyoid muscle (*MH*) and submandibular gland fossa (*SMF*). The *arrows* show the right mandibular canal. Note that the soft tissue contrast of CBCT is inadequate to differentiate the musculature of the floor of the mouth (*EOR* external oblique ridge, *IOR* internal oblique ridge or mylohyoid line)

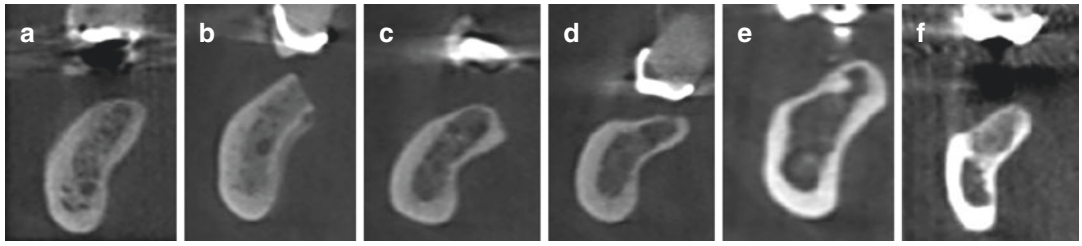

Fig. 10.44 Posterior right mandibular cross sections of the edentulous molar region from six different patients (**a**–**f**). Note the marked lingual undercuts in all cases (submandibular fossa). The tooth-bearing part of the mandibular bone rarely remains unchanged after tooth loss

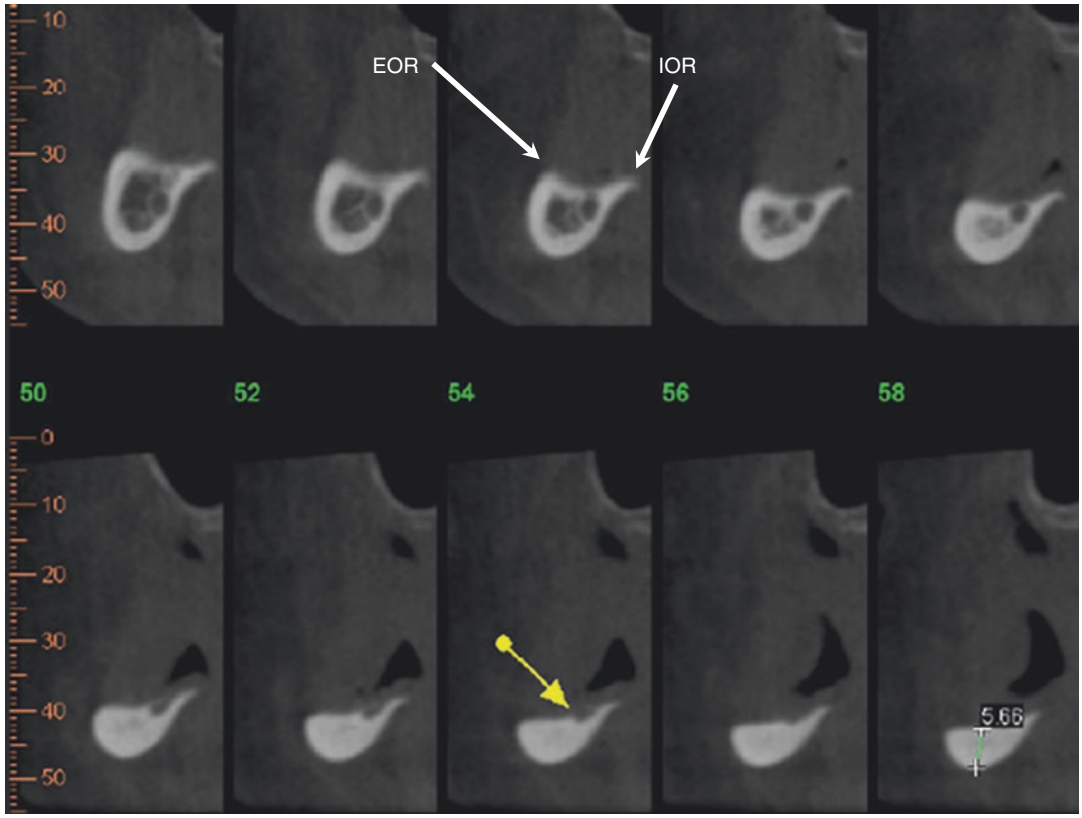

Fig. 10.45 Sequential trans-axial images at 1 mm intervals in a patient with long-term complete mandibular edentulousness showing severe atrophy of the edentulous alveolar bone in the right posterior mandible. The *yellow arrow* points out the right mental foramen which exits on the crest of the ridge. In fact no alveolar ridge is identified—the alveolar bone was at the level of the floor of the mouth. (*EOR* external oblique ridge, *IOR* internal oblique ridge)

the edentulous alveolar ridge which in turn may compromise future implant treatments.

Kottal et al. (2006) report that the angulation of the mandibular alveolar bone may deviate up to 30° from the favorable dental implant insertion path. Moreover, they found that the edentulous alveolar bone in the vast majority of the potential implant sites in their sample deviated

from 10° to 30° from the preferred implant insertion path determined for optimal restoration and function.

The thickness of the cortical bone as well as the trabecular pattern of the cancellous bone are also shown in the mandibular cross sections. A number of investigators have attempted to associate this pattern to certain levels of "bone quality" (Angelopoulos and Aghaloo 2011).

Mandibular Canal

The mandibular (MC) or inferior alveolar (IAC) canal presents as a major anatomical limitation for the placement of implants in the posterior mandible. It contains the inferior alveolar nerve (IAN), artery, and vein. The MC is tube-like structure that runs the entire length of the body of the mandible, almost parallel to the inferior border and usually located within the lower third of the body. Its posterior opening on the lingual aspect of the ramus, the mandibular foramen, is the entry point of the IAN (Fig. 10.46).

The IAN is a branch of the mandibular nerve (V3) and provides sensory innervation to the mandibular bone, teeth, the lower lip, and partially the gingivae of the anterior teeth. In cross-sectional images, the canal is visualized as a well-defined, small, most often round, low density area which is frequently surrounded by a high density border. The presence of the high density outline is dependent upon the canal's cortication. As a result, the MC is not always well visualized (Fig. 10.47). Carter and Keen (1971) and Wuehrman and Manson-Hing (1981) agreed that the occurrence of "not visible" mandibular canals is related to the fact that the inferior alveolar bundle is not always surrounded by an ossified canal. Stella and Tharanon (1990) related the reliability and accuracy of diagnostic imaging to the visibility of the mandibular canal.

The intramedullary course of the MC may also vary. Although the MC is frequently identified closer to the lingual mandibular cortex, this should not be taken for granted. The development of teeth as well as pathological entities in the posterior mandible may displace the MC and affect the presence and extent of cortication (Fig. 10.48).

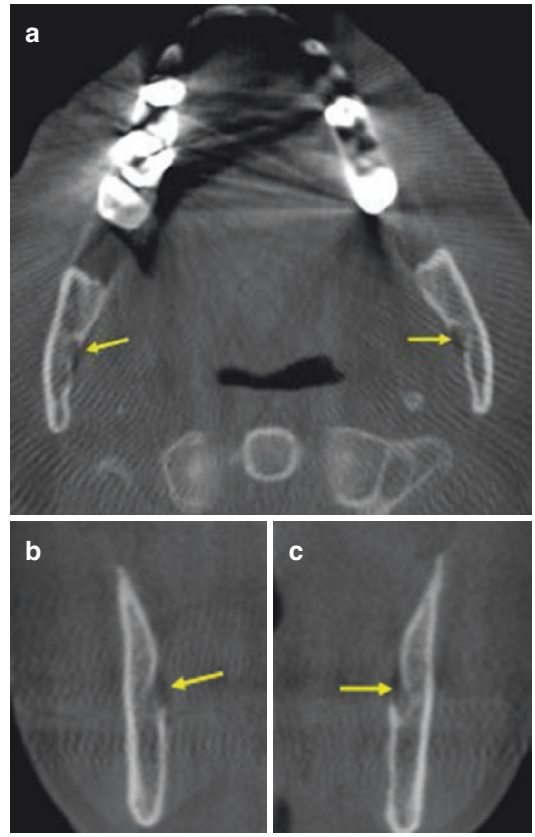

Fig. 10.46 Axial image (**a**) at the level of the mandibular rami and coronal cross-sectional images at the level of the *right* (**b**) and *left* (**c**) ascending rami. The *arrows* indicate the mandibular foramina, bilaterally, entry point of the IAN into the MC

Accessory branches of the IAN (other than its terminal branch) may sometimes emerge through the mandibular bone as smaller canals (Fig. 10.49).

Mental Foramen

The IAN perforates the buccal cortical plate of the mandible as the "mental nerve," through a small opening, the mental foramen. The mental foramen is located in the periapical region of the second premolar; however, there is considerable anatomic variability in location. It is best visualized in the cross-sectional images of the mandible (premolar region) as a variable in shape and size break in the continuity of the

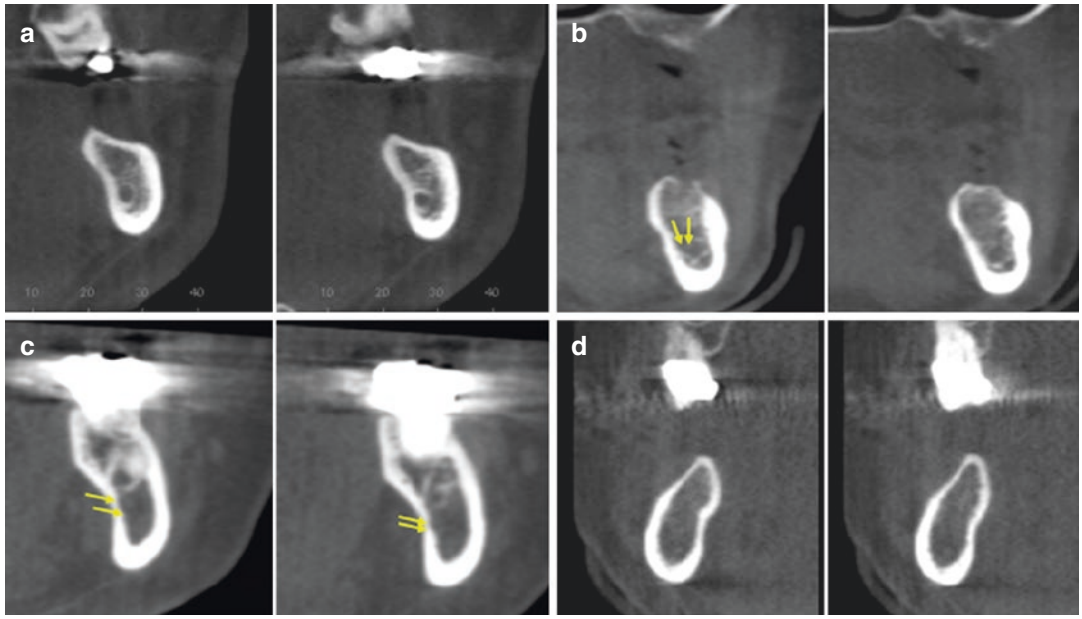

Fig. 10.47 The visualization of the mandibular canal is dependent upon the cortication of its borders. Adjacent sequential trans-axial images of corticated, easily visualized (**a**), partially corticated, well visualized (**b**), not corticated, poorly visualized (**c**) and not corticated non-visible (**d**) inferior alveolar canal. Note that the location of the inferior alveolar canal can be estimated when it grooves the internal margin of the lingual cortical plate—"niche sign" (**c**)

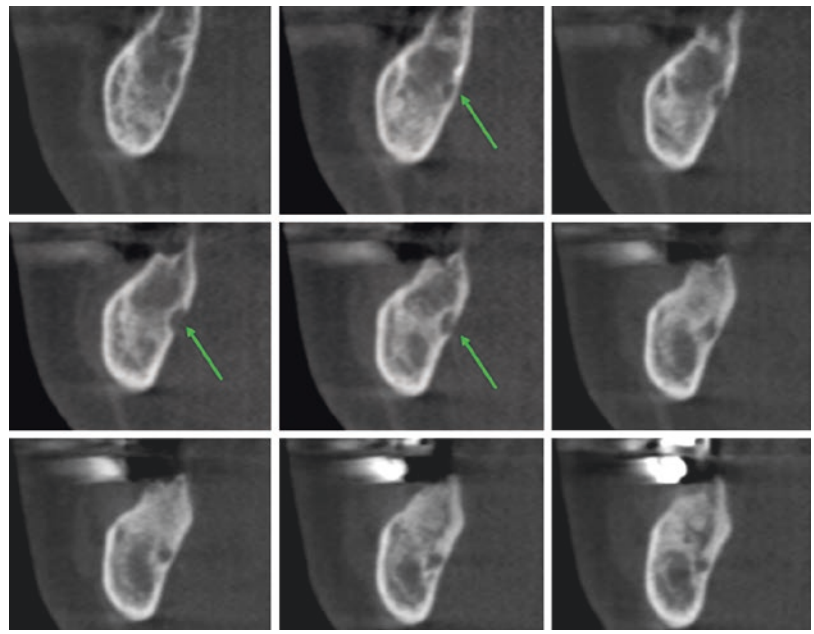

Fig. 10.48 Series of sequential 1 mm interval trans-axial sections showing the mandibular canal grooving and, in some areas, perforating the lingual cortex, exposed to the submandibular space

buccal cortex, in a small distance from the apices of the premolars (Fig. 10.50). The mental foramen represents a clear change of direction of a large part of the sensory fibers of the IAN which exit the mandibular canal. As a result, it may appear as a short tube-like structure, itself.

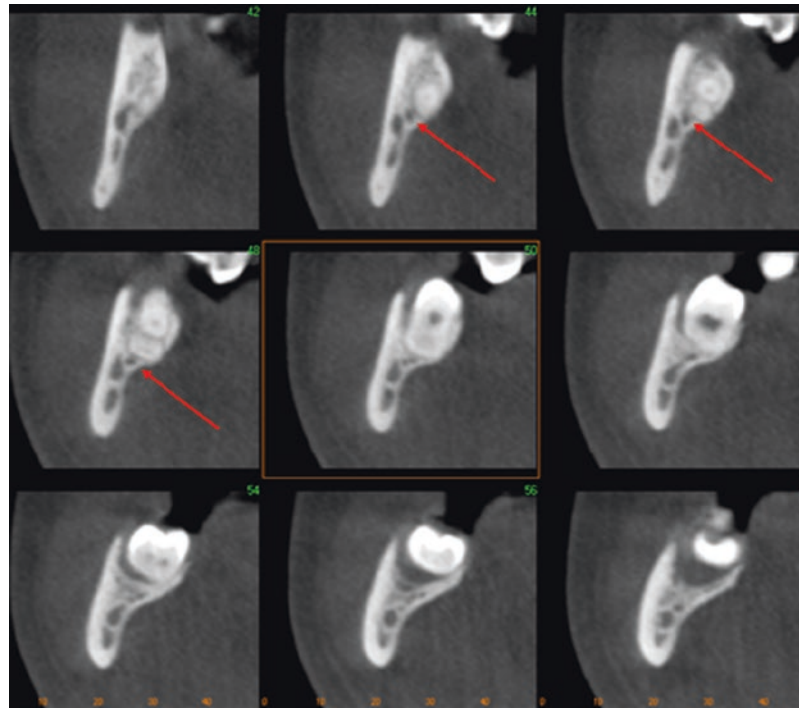

Fig. 10.49 Series of sequential 1 mm interval trans-axial sections showing the position of an impacted right mandibular third molar and its relationship to the inferior alveolar canal. Note the origin of a small accessory branch of the MC (*arrows*). Although the MC itself is located inferior and at some distance from the roots of the tooth, the accessory branch is in contact with the root

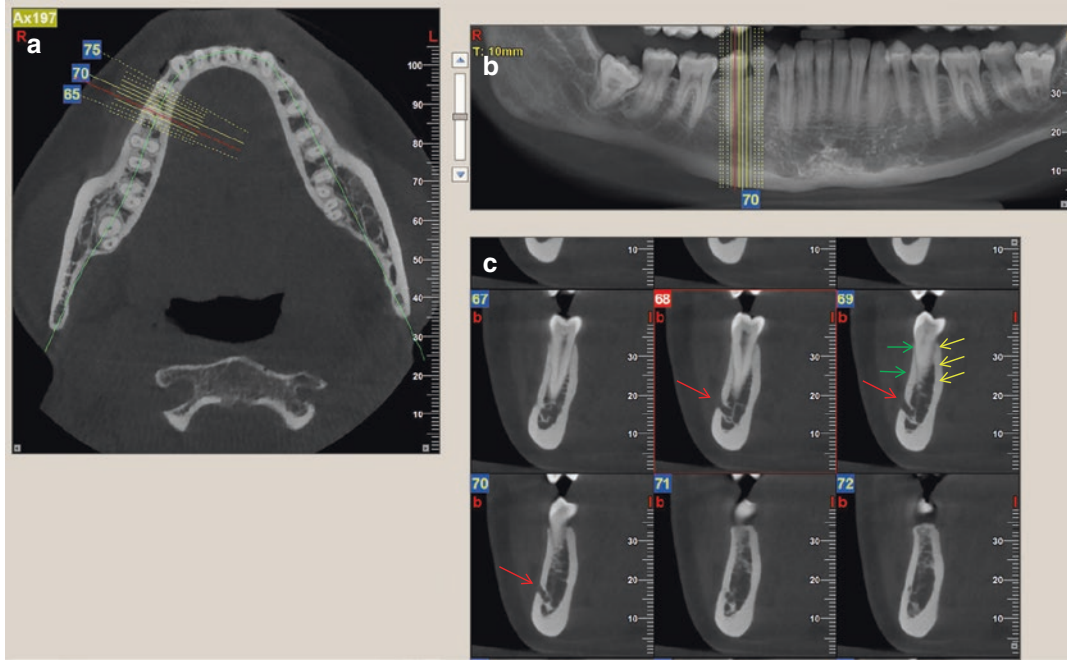

Fig. 10.50 Axial (**a**), reformatted panoramic (**b**), and serial cross-sectional (**c**) images of the premolar region of the mandible illustrating the mandibular alveolar process and relevant neighboring anatomical structures. These images depict alveolar bone height and width, buccal (*green arrows*) and lingual (*yellow arrows*) cortices and the mental foramen (*red arrows*). In this example, the mental foramen exits low through the inferior third of the buccal cortical plate

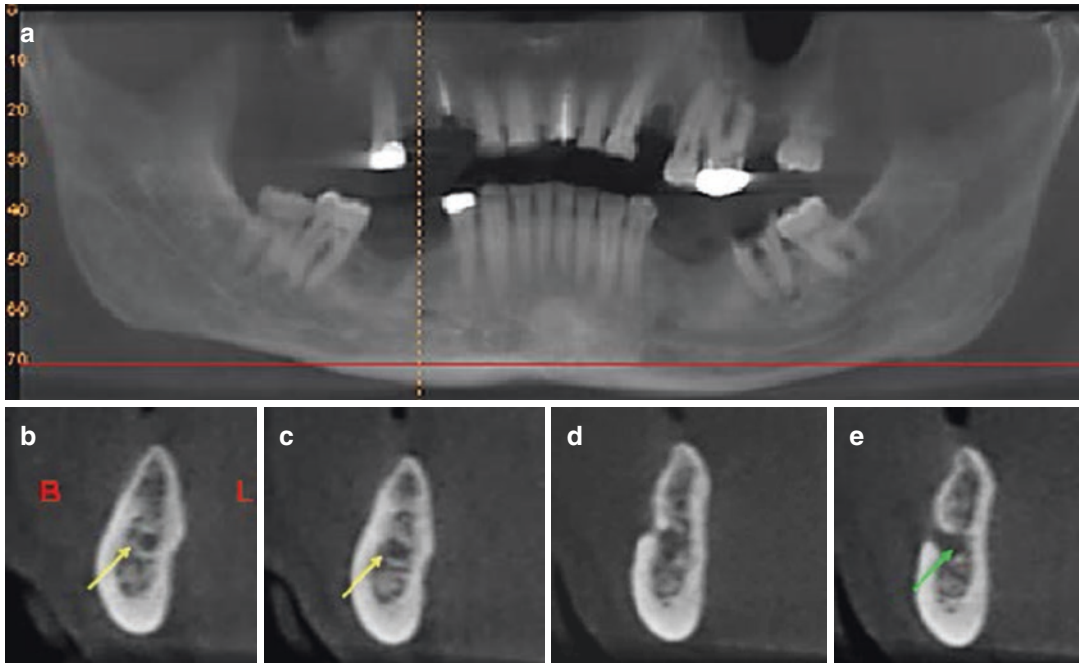

Fig. 10.51 Reformatted panoramic (**a**) and cross-sectional images (**b–e**) in the region mandibular of right premolars (*yellow dotted line* on panoramic image). The *yellow arrows* show the right mandibular canal and the *green arrow* shows the mental foramen as it exits high through the middle third of the buccal cortex of the mandible

The angle at which the mental foramen emerges through the buccal cortex as well as the level relative to the alveolar height is variable (Figs. 10.51 and 10.52).

After the mental branch exits through the mental foramen, the terminal branch of the IAN continues an intra-osseous course towards the midline of the mandible as the *incisive branch*, providing sensory innervation to the anterior mandibular teeth. A smaller diameter osseous canal may be seen anterior to the mental foramen (Fig. 10.53).

Proper knowledge and utilization of the tools available for image reformatting will assist in the identification of vital anatomical structures such as the MC when their location is unclearly visible. The use of consecutive thin sagittal sections of the posterior mandible (in the areas of interest) or consecutive panoramic sections may be of great assistance, if the MC is not visualized in the corresponding cross-sectional images. Abrahams and Levine (1990) introduced the concept of MC canal triangulation if the MC is not visible in some of the sections of interest. This concept includes proper use of the metric scales that often are provided on the borders of almost all types of sections. So, if the MC is visible in one image series (e.g., panoramic sections), the height of the superior border of the MC could be marked in the metric scale next to the panoramic sections; next this metric reading could be transferred to the corresponding scale in the cross-sectional images. In this way, a fairly accurate estimate of the mandibular bone height could be provided even if the MC is not visible in some of the sectional images. This concept is far more easily applicable to the CBCT images due to the interactivity that CBCT software offers (Fig. 10.54).

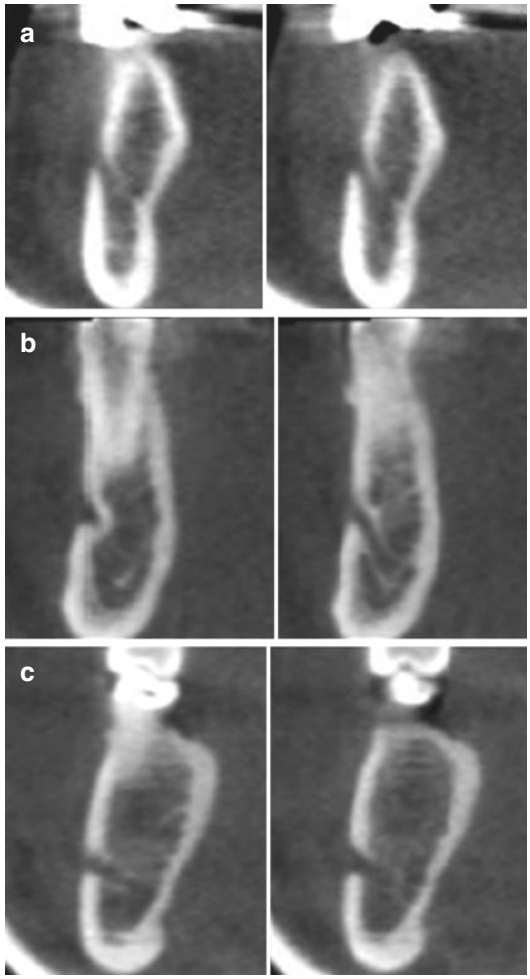

Fig. 10.52 Cross-sectional images in the area of mandibular premolars from three patients (**a**–**c**). There is considerable variation as far as the size and the opening angle of the mental foramen between different individuals ranging from very steep upwards angle of opening of the mental foramen (**a**, **b**) to an almost flat opening angle (**c**)

10.4 The Oral Cavity and Oropharynx

Because of their proximity and continuity, the oral cavity and oropharynx can be considered as a single anatomical unit.

The oral cavity/oropharynx is a semispherical common pathway which serves as the first component of the alimentary and respiratory tracts. It is bound by the lips and teeth (anterior), the teeth and cheeks (laterally), the tongue and the floor of the mouth (inferior), the hard and soft palate (superior), and the pharyngeal wall (posterior). It is almost entirely comprised of soft tissue elements and it is lined by mucosa. On CBCT imaging the surface outlines of these elements are often represented (Figs. 10.55, 10.56, and 10.57).

Shape alterations of the oropharynx may reflect developing pathology in its borders. Unfortunately the poor soft tissue contrast of CBCT is inadequate for soft tissue pathology diagnosis; however, due to the high contrast between air and the surrounding soft tissues, recognition of shape discrepancies or asymmetries in the upper airway may elevate suspicion for disease. For example, pathologic enlargement of superficial glandular tissues in the oral cavity (e.g., palatine, pharyngeal and lingual tonsils, and the tongue) may result in an alteration of the shape of the upper airway and may suggest pathology (Fig. 10.58). In addition, tissues that mineralize or produce calcified material as a result of pathology (e.g., sialoliths, or tonsilar calcifications) may be readily recognized with CBCT (Fig. 10.59).

10.5 The Nasopharynx

The nasopharynx is a short tube-like structure and the most superior section of the upper airway (Fig. 10.60). It is bounded by the soft palate caudally and the mucosal lining of the base of the sphenoid bone cranially. It extends posteriorly to the pharyngeal tonsils, adjacent the upper cervical spine, whereas anteriorly it extends to the posterior choanae (the posterior openings of the nasal cavity) and enters the nasal cavity. The lateral borders of the nasopharynx are formed by the pharyngotympanic or eustatian tube which connects the nasopharynx to the inner ear, the torus tubarius (the cartilaginous end of the eustachian tube), and the lateral pharyngeal recess (fossa of Rosenmuller) on either side.

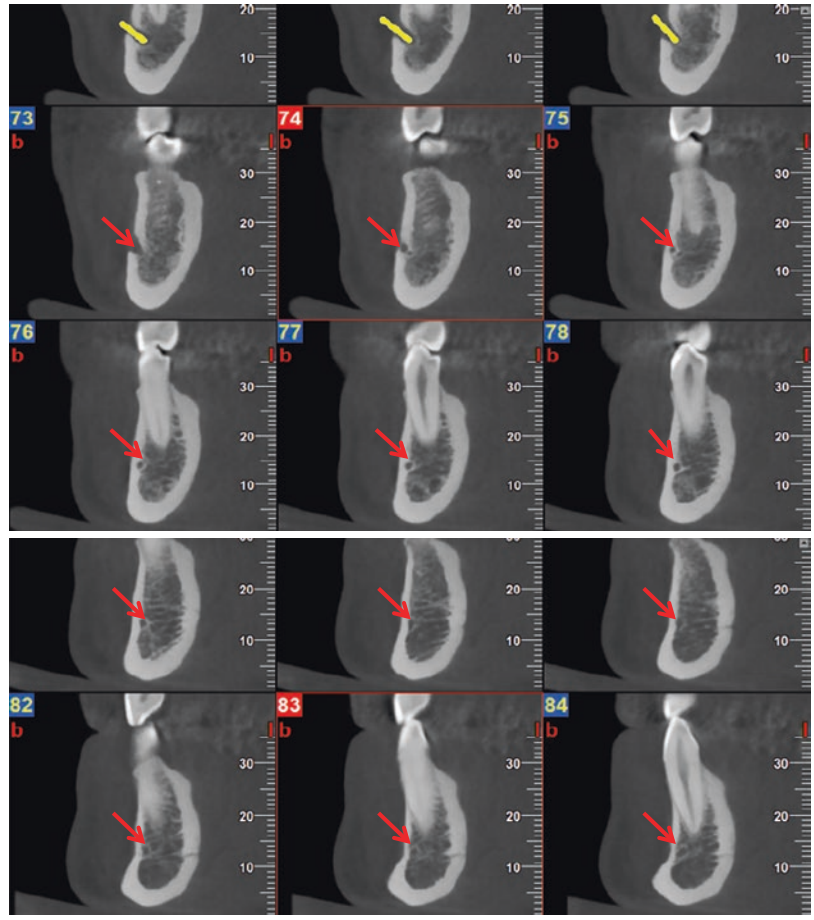

Fig. 10.53 Sequential 1 mm interval transaxial images demonstrating a low density, round structure in the mandibular symphyseal region anterior to the mental foramen (*red arrows*) containing the incisive branch of the inferior alveolar neurovascular bundle

The eustachian tube originates from the nasopharynx as a collapsed narrow opening just posterior to the medial pterygoid plate and follows a lateral/superior course towards the auditory apparatus. Its posterior wall is the torus tubarius (or cushion of the tube); this is a finger-like projection which borders the lateral pharyngeal recess (fossa of Rosenmuller) from the eustachian tube. The fossa of Rosenmuller is of special significance since it is the most frequent site of nasopahryngeal carcinoma in older individuals, the most common nasopahryngeal malignancy.

The various soft tissue projections and recesses in the nasopharynx result in a characteristic "star" shape observed in axial sections (Fig. 10.60). Therefore, alterations in this shape may be associated with developing disease and require referral and further investigation (Fig. 10.61).

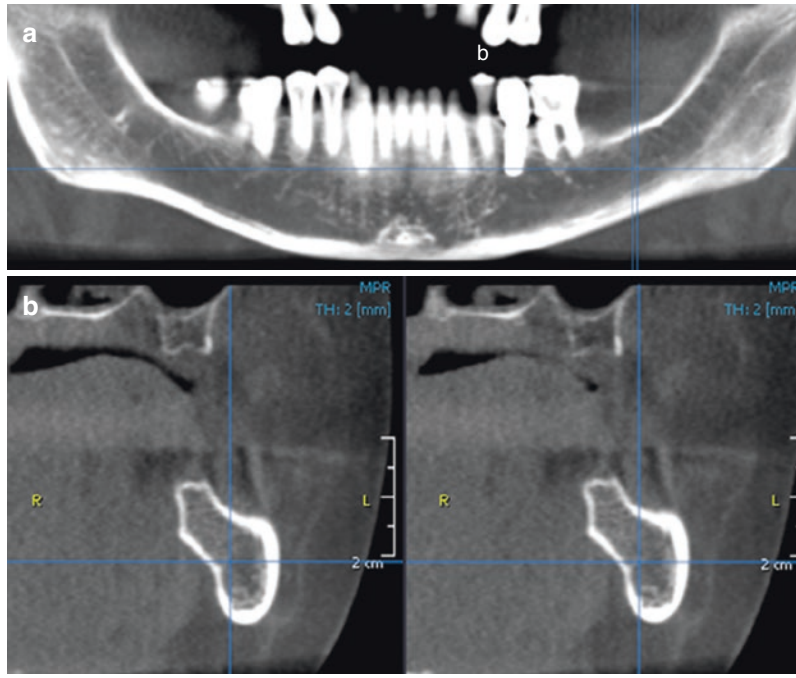

Fig. 10.54 Example of the use of triangulation to localize the inferior alveolar canal. Metric scales or reference lines displayed on various images can assist to "triangulate" the location of the MC. In this example the MC is fairly well visualized in the left mandibular edentulous area in the panoramic section (**a**). The two *vertical lines* represent the location of the two cross sections (**b**). The *horizontal blue* reference line corresponds to the axial mandibular section at this level which is at the same level in both panoramic and cross-sectional cuts. Consequently, if we move the *horizontal line* to coincide with the superior border of the MC, this will be transferred accordingly to the respective cross sections. The "cross-hair" point between the *horizontal* and *vertical* reference lines depicts the same anatomical location irrespective of the type of sectional images

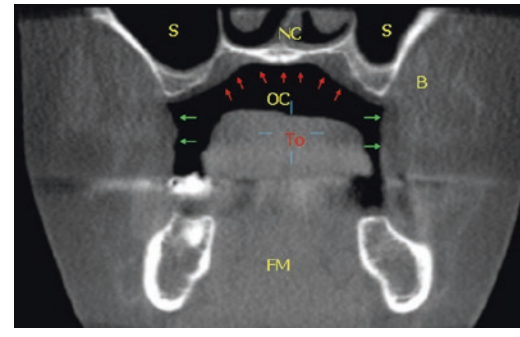

Fig. 10.55 Coronal section through a posterior edentulous maxilla and mandible Note the severe atrophy of the maxillary alveolar bone bilaterally. The image shows the spatial relationships of the bony anatomic boundaries and soft tissue contents of the oral cavity including the nasal cavity (*NC*), oral cavity (*OC*), buccal soft tissues of the cheeks (*B*), maxillary sinus (*S*), tongue (*To*) and floor of mouth (*FM*). The red arrows show the hard palate and the green arrows indicate the patient's cheeks

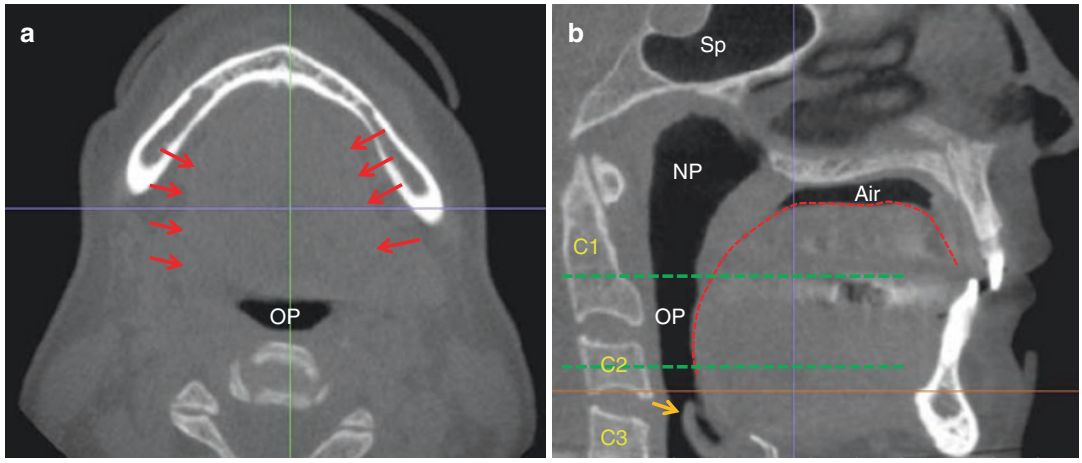

Fig. 10.56 Axial section at the level of the floor of the mouth (**a**) and midsagittal (**b**) section illustrating the lower borders of the oral cavity; tongue (*red arrows*) and the vertical relationship between the oropharynx (*OP*) and nasopharynx (*NP*). The *curved dotted red line* outlines the dorsum of tongue. (*orange arrow* epiglottis, *C1*, *C2*, *C3*, respective cervical vertebrae

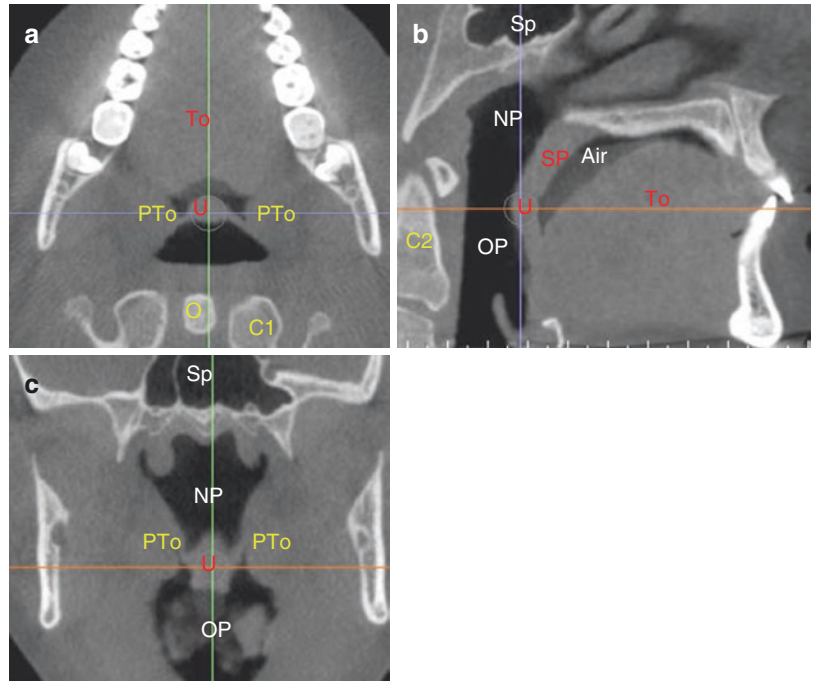

Fig. 10.57 Axial orthogonal section (**a**) at the level of the border between oropharynx/nasopharynx illustrating the lateral borders of the oral cavity/oropharynx. Midsagittal orthogonal section (**b**) showing the vertical relationship between the oropharynx (OP) and nasopharynx (NP) as well as the shape transition of these cavities. Coronal section through the upper airway (**c**) showing the lateral borders of the OP and NP and their shape changes in the coronal plane (*PTo* palatine tonsils, *To* tongue, *SP* soft palate, *U* uvula, *Sp* sphenoid sinus, *O* odontoid process of C2)

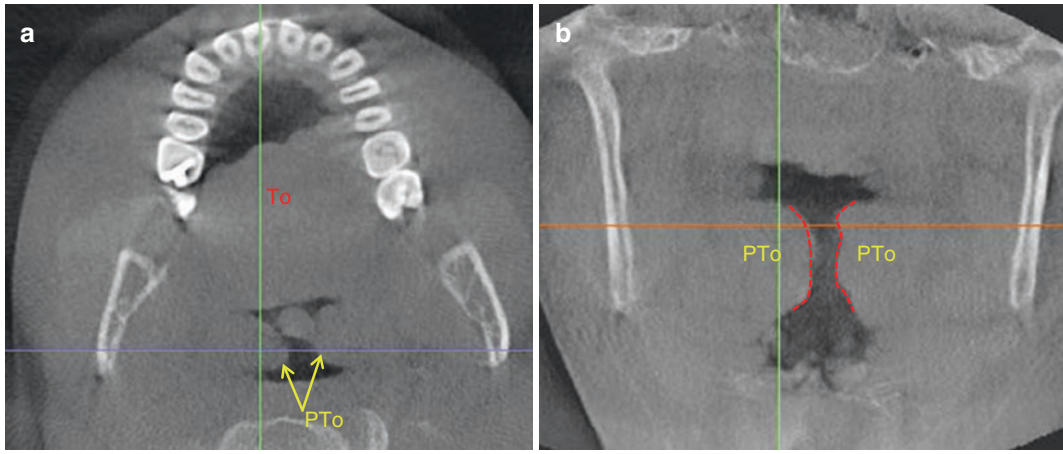

Fig. 10.58 Axial (**a**) CBCT image at the level of the maxillary teeth and coronal (**b**) CBCT image of the oropharynx showing severe narrowing of the airway by bilateral soft tissue masses, projecting into the lumen of the airway. The location and appearance of these masses is consistent with bilateral palatine tonsillar hypertrophy (*PTo* palatine tonsils, *To* tongue)

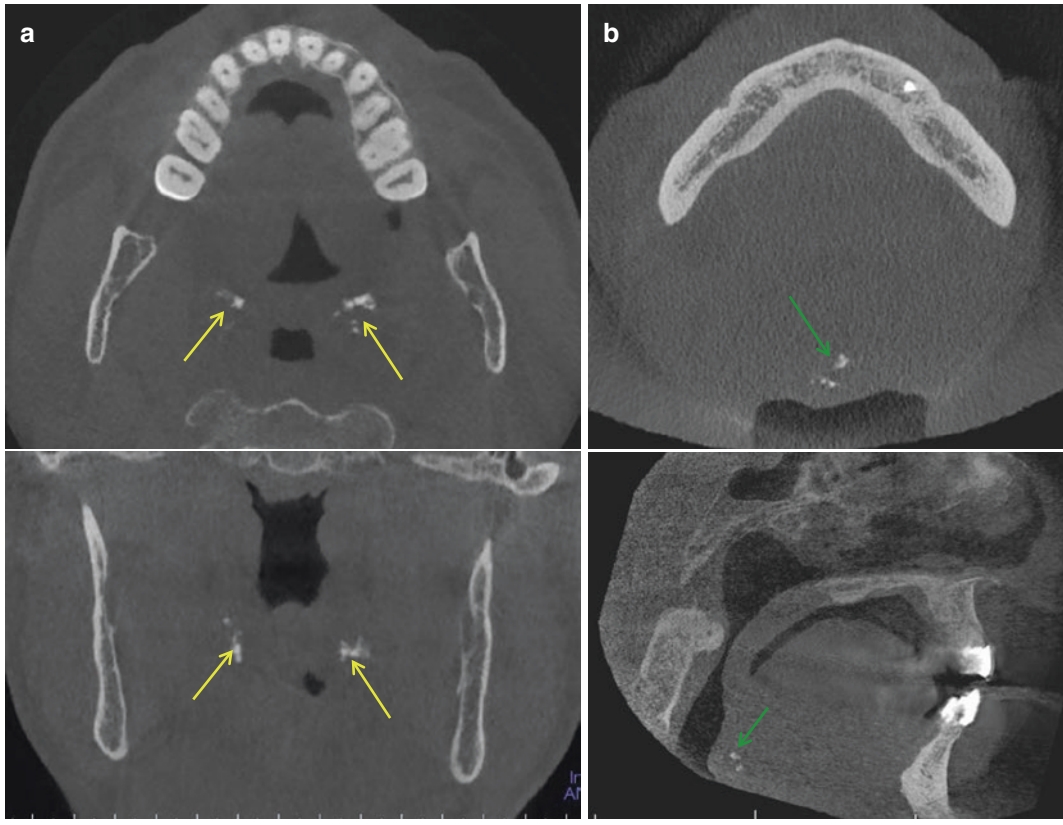

Fig. 10.59 Axial (*upper image*) and coronal (*lower image*) sections of the oropharynx of an individual (**a**) depicting lateral tonsilar calcifications in the palatine tonsils (*yellow arrows*) and axial (*upper image*) and midsagittal (*lower image*) sections of the oropharynx of a second individual (**b**) with calcifications in the lingual tonsils (*green arrows*). In both individuals the tonsillar tissue is not identified, however the presence and morphology of calcifications at these locations is highly suggestive of tonsilar mineralizations

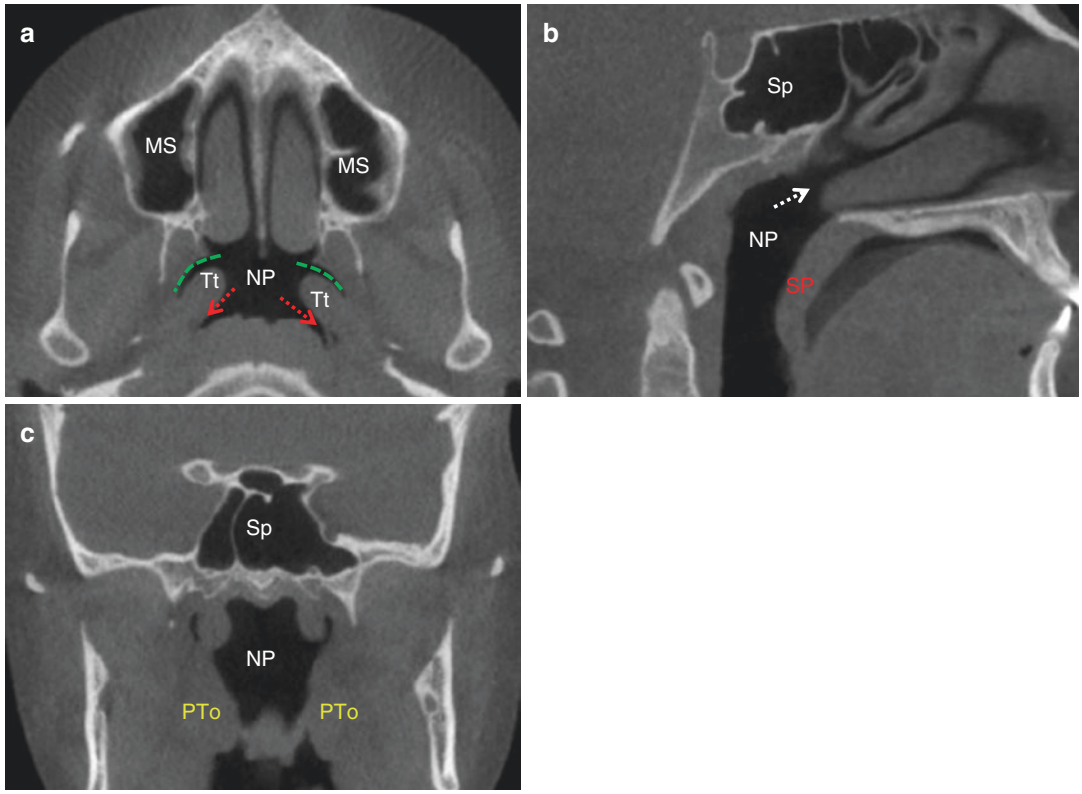

Fig. 10.60 Axial (**a**), midsagittal (**b**), and coronal (**c**) CBCT images of the nasopharynx (NP) demonstrating normal shape and size. (*green dotted line* the Eustachian tube, *Tt* the torus tubarius, *dashed red arrows* lateral pharyngeal recess or fossa of Rosenmuller, *MS* maxillary sinus; *Sp* sphenoid sinus, *PTo* palatine tonsils)

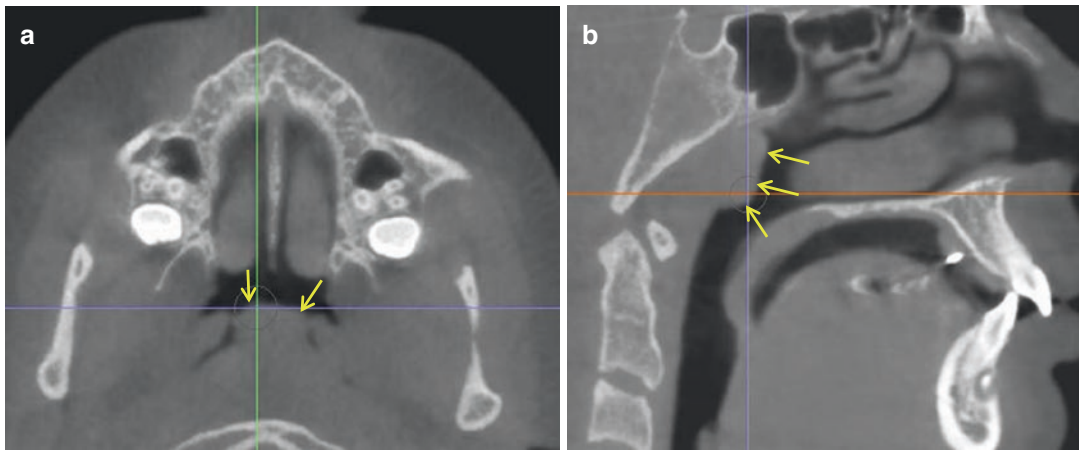

Fig. 10.61 Axial (**a**) and midsagittal (**b**) CBCT images of the nasopharynx showing a large soft tissue projection originating from the posterior wall of the nasopharynx, markedly narrowing the nasopahryngeal airway and altering its characteristic "star" shape. The imaging appearance is suggestive of posterior pharyngeal tonsilar hypertrophy (hypertrophic adenoids), however referral to an otolaryngologist should be considered based on clinical and medical history

Acknowledgments The concept of dividing the panoramic image into regions or zones for radiologic assessment is introduced courtesy of Dr. Bruno Azevedo.

References

Abrahams JJ, Levine B (1990) Expanded applications of DentaScan (multiplanar computer-ized tomography of the mandible and maxilla). Int J Periodontics Restorative Dent 10:464–471

Angelopoulos C (2008) Cone beam tomographic imaging anatomy of the maxillofacial region. Dent Clin N Am 52:731–752

Angelopoulos C (2014) Anatomy of the maxillofacial region in the three planes of section. Dent Clin N Am 58:497–521

Angelopoulos C, Aghaloo T (2011) Imaging technology in implant diagnosis. Dent Clin N Am 55:141–158

Carter RB, Keen EN (1971) The intramandibular course of the inferior alveolar nerve. J Anat 108(Pt 3):433–434

Chapnick L (1980) A foramen on the lingual of the mandible. J Can Dent Assoc 46:444–445

de Oliveira GJPL, Abdala MA, Nary-Filho H, Sakakura CE, Garcia VG, Leite FC (2017) Tomographic evaluation of prevalence, position, and diameter of the intraosseous branch of the posterior superior alveolar artery in fully edentulous individuals. J Craniofac Surg 28:279–283

Fernández-Alonso A, Suárez-Quintanilla JA, Rapado-González O, Suárez-Cunqueiro MM (2015) Morphometric differences of nasopalatine canal based on 3D classifications: descriptive analysis on CBCT. Surg Radiol Anat 37:825–833

Hafeez NS, Ganapathy S, Sondekoppam R, Johnson M, Merrifield P, Galil KA (2015) Anatomical variations of the greater palatine nerve in the greater palatine canal. J Can Dent Assoc 81:f14

Kalpidis CD, Setayesh RM (2004) Hemorrhaging associated with endosseous implant place-ment in the anterior mandible: a review of the literature. J Periodontol 75:631–645

Kottal S, Angelopoulos C, Parris V, Thomas S (2006) Classification of Edentulous Posterior Mandible by Means of Alveolar Ridge Angulation. Abstract book of the 10th European Congress of Dentomaxillofacial Radiology. p. 169 (Published abstract).

Wuehrman AH, Manson-Hing LR (1981) Dental Radiology, 5th ed. Mosby, St. Louis.

Monje A, González-García R, Monje F, Chan HL, Galindo-Moreno P, Suarez F, Wang HL (2015) Microarchitectural pattern of pristine maxillary bone. Int J Oral Maxillofac Implants 30:125–132

Scarfe WC, Farman AG, Sukovic P (2006) Clinical applications of cone-beam computed tomography in dental practice. J Can Dent Assoc 72(1):75–80

Scarfe WC, Farman AG, Levin MD, Gane D (2010) Essentials of maxillofacial cone beam computed tomography. Alpha Omegan 103:62–67

Shiller WR, Wiswell OB (1954) Lingual foramina of the mandible. Anat Rec 119:387–390

Stella JP, Tharanon W (1990) A precise radiographic method to determine the location of the inferior alveolar canal in the posterior edentulous mandible: implications for dental implants. Part 1: technique. Int J Oral Maxillofac Implants 5:15–22

Tepper G, Hofschneider UB, Gahleitner A, Ulm C (2001) Computed tomographic diagnosis and localization of bone canals in the mandibular interforaminal region for prevention of bleeding complications during implant surgery. Int J Oral Maxillofac Implants 16:68–172

White SC, Rudolph DJ (1999) Alterations of the trabecular pattern of the jaws in patients with osteoporosis. Oral Surg Oral Med Oral Pathol Oral Radiol Endod 88:628–635